

DoCoFL: Downlink Compression for Cross-Device Federated Learning

Ron Dorfman^{*1,2}, Shay Vargaftik¹, Yaniv Ben-Itzhak¹ and Kfir Y. Levy^{†2}

¹VMware Research

²Viterby Faculty of Electrical and Computer Engineering, Technion

Abstract

Many compression techniques have been proposed to reduce the communication overhead of Federated Learning training procedures. However, these are typically designed for compressing model updates, which are expected to decay throughout training. As a result, such methods are inapplicable to downlink (i.e., from the parameter server to clients) compression in the cross-device setting, where heterogeneous clients *may appear only once* during training and thus must download the model parameters.

In this paper, we propose a new framework (DoCoFL) for downlink compression in the cross-device federated learning setting. Importantly, DoCoFL can be seamlessly combined with many uplink compression schemes, rendering it suitable for bi-directional compression. Through extensive evaluation, we demonstrate that DoCoFL offers significant bi-directional bandwidth reduction while achieving competitive accuracy to that of FedAvg without compression.

1 Introduction

In recent years, there has been an increasing interest in federated learning (FL) as a paradigm for large-scale machine learning over decentralized data (Konečný et al., 2016a; Kairouz et al., 2021). FL enables organizations and/or devices, collectively termed *clients*, to jointly build better and more robust models by relying on their collective data and processing power. Importantly, the FL training procedure occurs without exchanging or sharing client-specific data, thus ensuring some degree of privacy and compliance with data access rights and regulations (e.g., the General Data Protection Regulation (GDPR) implemented by the European Union in May, 2018). Instead, in each round, clients perform local optimization

*Work done while at VMware Research. Corresponding author: rdorfman@campus.technion.ac.il.

†A Viterbi Fellow.

using their local data and send only model updates to a central coordinator, also known as the *parameter server* (PS). The PS aggregates these updates and updates the global model, which is then utilized by the clients in subsequent rounds.

One of the main challenges in FL is the communication bottleneck introduced during the distributed training procedure. To illustrate this bottleneck, consider the following example of a real FL deployment presented by McMahan et al. (2022): their training involves a small neural network with 1.3 million parameters; in each round there are 6500 participating clients; and the model is trained over 2000 rounds. A simple calculation shows that the total required bandwidth to and from the PS during this training is ≈ 61.5 TB. Since modern machine learning models have many millions (or even billions) of parameters and we might have more participants, FL may result in excessive communication overhead.

To deal with this overhead, many bandwidth reduction techniques have been proposed. These include taking multiple (rather than a single) local optimization steps (McMahan et al., 2017), quantization techniques (Seide et al., 2014; Alistarh et al., 2017; Wen et al., 2017; Bernstein et al., 2018a,b; Karimireddy et al., 2019; Jin et al., 2020; Shlezinger et al., 2020), low-rank decomposition (Vogels et al., 2019), sketching (Ivkin et al., 2019; Rothchild et al., 2020), and distributed mean estimation (Lyubarskii and Vershynin, 2010; Suresh et al., 2017; Konečný and Richtárik, 2018; Safaryan et al., 2022; Vargaftik et al., 2021, 2022). However, as we detail in §2, all these techniques do not support downlink compression, i.e., from the PS to the clients, in the cross-device setup in which new and heterogeneous clients may participate at each round and thus must download the model parameters. This is in contrast to the cross-silo setup in which the PS can compress and send a global update (i.e., clients’ aggregated update) to all silos.

To the best of our knowledge, there are only a handful of works that consider bi-directional compression, i.e., compression from the clients to the PS and vice versa, (Tang et al., 2019; Zheng et al., 2019; Liu et al., 2020; Philippenko and Dieuleveut, 2020, 2021; Grunkowska et al., 2022) and all rely on per-client memory mechanism. Thus, these solutions target either distributed learning or cross-silo FL (possibly with partial but recurring participation), and they are not suitable for cross-device FL, where a client may appear only a handful of times, or even just once, during the entire training procedure.

It is important to stress that the significance of bi-directional bandwidth reduction for cross-device FL goes far beyond cost reduction, energy efficiency, and carbon footprint considerations. In fact, inclusion, fairness, and bias are at the very heart of cross-device FL as, according to recent sources (Sumra, 2020; Howdle, 2022), the price of a wireless connection and its quality admits differences of orders of magnitude among countries. This may prevent large populations from contributing to cross-device FL training due to costly and unstable connectivity, resulting in biased and less accurate models.

Accordingly, in this work we introduce DoCoFL, a novel downlink compression framework specifically designed for cross-device FL. Importantly, it operates independently of many up-link compression techniques, making it suitable for bi-directional compression in cross-device setups.

The primary challenge addressed by DoCoFL is that clients must download model parameters (i.e., weights) instead of model updates. Unlike updates, which are proportional to gradients and thus their norm is expected to decrease during training, the model parameters do not decay, making it undesirable to use low-bit compression methods. As a result, and since clients can only download the model weights during their designated participation round, this can lead to a network bottleneck for low-resourced clients.

To address this bottleneck, DoCoFL decomposes the download burden by utilizing previous models, referred to as *anchors*, which clients can download prior to their participation round. Then, at the designated participation round, clients only need to download the correction, i.e., the difference between the updated model and the anchor. As the correction is proportionate to the sum of previous updates, it is expected to decay, allowing for the use of low-bit compression methods. To ensure the correction term and PS memory footprint remain manageable, the available anchors are updated periodically. This approach reduces the amount of bandwidth required by the clients *online* (i.e., at their participation round). To reduce the overall downlink bandwidth usage, we further develop and utilize an efficient anchor compression technique with an appealing bandwidth-to-accuracy tradeoff.

Contributions. We summarize our contributions below,

- We propose a new framework (DoCoFL) that both enlarges the time window during which clients can obtain the model parameters and reduces the total downlink bandwidth requirements for cross-device FL.
- We show that DoCoFL provably converges to a stationary point when not compressing anchors and give an asymptotic convergence rate.
- We design a new compression technique with strong empirical results, which DoCoFL uses for anchor compression and can be of independent interest. We provide the theoretical intuition and empirical evidence for why DoCoFL with anchor compression works.

Finally, we show over image classification and language processing tasks that DoCoFL consistently achieves model accuracy that is competitive with an uncompressed baseline, namely, FedAvg (McMahan et al., 2017) while reducing bandwidth usage in both directions by order of magnitude.

2 Background and Related Work

In this section, we overview mostly related work and detail the challenges in designing a bi-directional bandwidth reduction framework for cross-device FL.

2.1 Uplink vs. Downlink

In the context of FL, uplink (i.e., client to PS) and downlink (i.e., PS to client) compression are inherently different and should not be treated in the same manner. In particular, many recent uplink compression solutions (e.g., [Konečný et al. \(2016b\)](#); [Alistarh et al. \(2017\)](#); [Ramezani-Kebrya et al. \(2021\)](#)) partially rely on two properties to obtain their effectiveness:

Averaging. A fundamental property in having many clients sending their compressed gradients for averaging at the PS is that if their estimation errors are independent and unbiased, then the error in estimating their true mean by calculating their estimations' mean is decreasing linearly with respect to the number of clients. Thus, having more clients in a training round allows for more aggressive and more accurate compression.

Error Decay. The effect of increased variance in the global gradient estimation, unlike in the model parameters, can be compensated by decreasing the learning rate and diminishes as the training process continues. Also, having the global gradient norm decay is expected and is the optimality condition in non-convex gradient-based optimization.

For downlink compression, we immediately lose the averaging property since, by design, there is only one source with whom the clients communicate, namely, the PS. Regarding the error decay property, we must further distinguish between different FL setups as described next.

2.2 Cross-silo vs. Cross-device

FL can be divided into two types based on the nature of the participating clients ([Kairouz et al. \(2021\)](#), Table 1).

Silos. In cross-silo FL, the clients are typically assumed to be active throughout the training procedure and with sufficient compute and network resources. Silos are typically associated with entities such as hospitals that jointly train a model for better diagnosis and treatment ([Ng et al., 2021](#)) or banks that jointly build better models for fraud and anomalous activity detection ([Yang et al., 2019](#)).

Indeed, silos allow for the design of efficient compression techniques that rely on client persistency and per-client memory mechanisms that are used for, e.g., compressing gradient differences, employing error feedback, and learning control variates ([Alistarh et al., 2018](#); [Karimireddy et al., 2020](#); [Philippenko and Dieuleveut, 2020](#); [Gorbunov et al., 2021](#); [Richtárik et al., 2021](#)). While most of these techniques consider only uplink compression, some recent works target bi-directional compression utilizing the same property of using per-client memory and where a client *repeatedly* participates in all or some training rounds ([Tang et al., 2019](#); [Liu et al., 2020](#); [Philippenko and Dieuleveut, 2020, 2021](#); [Grunkowska et al., 2022](#)).

Table 1: Averaging and Error Decay in different setups.

		Averaging	Error Decay
Uplink		✓	✓
Downlink	Cross-silo	✗	✓
	Cross-device	✗	✗

Devices. In cross-device FL, clients are typically assumed to be heterogenous and not persistent to the extent that a client often participates in a *single* out of many thousands of training rounds. Also, in this setup, clients may often admit compute and network constraints. Devices are usually associated with entities such as laptops, smartphones, smartwatches, tablets, and IoT devices. A typical example of a cross-device FL application is keyboard completion for android devices (McMahan and Ramage, 2017).

Unlike in silos with full or partial but repeated participation, compression techniques for devices that appear only once or a handful of times cannot rely on having some earlier state for or on that device. This renders methods that rely on per-client memory or learned control variates unsuitable for cross-device FL. Indeed, recent gradient compression and distributed mean estimation techniques are designed for the cross-silo setup or only uplink compression in both setups (Konečný et al., 2016b; Alistarh et al., 2017; Suresh et al., 2017; Ramezani-Kebrya et al., 2021; Vargaftik et al., 2021, 2022; Safaryan et al., 2022).

2.3 Putting It All Together

As summarized in Table 1, differences in the clients’ nature and the compression direction (i.e., uplink vs. downlink) significantly affect the efficiency of bandwidth reduction techniques. In the considered setups, downlink compression is more challenging than uplink compression due to the lack of averaging and received considerably less attention in the literature. Moreover, for the cross-device setup, the problem is more acute due to not having error decay as well.

3 DoCoFL

In this section, we present DoCoFL. We start with describing our design goals, derived from the challenges outlined in the previous section, followed by a formal definition of the federated optimization problem. Then, in §3.1, we give intuition and introduce our framework. In §3.2, we detail about an important element of DoCoFL, namely, the client selection process employed by the PS. Finally, we provide a theoretical convergence result in §3.3.

Design Goals. Motivated by the discussion in the previous section, we aim at achieving two goals to deal with the low bandwidth and slow and unstable connectivity conditions that edge devices may experience:

1. *Enlarging the time window* during which a client can download the model weights from the PS.
2. *Reducing the bandwidth* consumption in the downlink direction.

Achieving both these goals will enable more heterogeneous clients to participate in the training process, which in turn may reduce bias and improve fairness.

Preliminaries. We use $\|\cdot\|$ to denote the L_2 norm and for every $n \in \mathbb{N}$, $[n] := \{1, \dots, n\}$. Let N be the number of clients participating in the federated training procedure. Each client $i \in [N]$ is associated with a local loss function f_i , and our goal is to minimize the loss with respect to all the clients, i.e., to solve

$$\min_{w \in \mathbb{R}^d} f(w) := \frac{1}{N} \sum_{i=1}^N f_i(w). \quad (1)$$

Unlike in standard distributed optimization or cross-silo FL with full or partial but repeated participation, in cross-device FL, only a subset of S clients participate in each optimization round and typically $S \ll N$ (e.g., S in the hundreds/thousands and N in many millions). Thus, clients are not expected to repeatedly participate in the optimization.

Since FL mostly considers non-convex optimization (e.g., neural networks), and global loss minimization of such models is generally intractable, we focus on finding an approximate stationary point, i.e., a point w for which the gradient norm $\|\nabla f(w)\|$ tends to zero.

For the purpose of formal analysis, we make a few standard assumptions, namely, that f is bounded from below by f^* , the local functions $\{f_i\}$ are β -smooth, i.e., $\|\nabla f_i(w) - \nabla f_i(u)\| \leq \beta \|w - u\|$, $\forall w, u \in \mathbb{R}^d$, and the access to every local function is done via a stochastic gradient oracle, i.e.,

Assumption 3.1. For any $w \in \mathbb{R}^d$, client i computes an unbiased gradient estimator $g^i(w)$ with bounded variance σ^2 , i.e.,

$$\mathbb{E}[g^i(w)] = \nabla f_i(w), \quad \mathbb{E} \|g^i(w) - \nabla f_i(w)\|^2 \leq \sigma^2. \quad (2)$$

Additionally, we assume that the dissimilarity of the local gradients is bounded, which effectively limits the level of client data heterogeneity. This assumption is standard in the context of distributed optimization algorithms (Karimireddy et al., 2020; Koloskova et al., 2020; Wang et al., 2020).

Assumption 3.2. There exist constants $G, B \in \mathbb{R}_+$ such that

$$\frac{1}{N} \sum_{i=1}^N \|\nabla f_i(w)\|^2 \leq G^2 + B^2 \|\nabla f(w)\|^2, \quad \forall w \in \mathbb{R}^d. \quad (3)$$

3.1 Overview

A naive approach to reduce bandwidth in the downlink direction is to apply some compression to the model weights and have all participating clients download the compressed weights. That is, in each round t , the participating clients $\mathcal{S}_t \subseteq [N]$ obtain a compressed version of the model weights $\hat{w}_t = \mathcal{C}_w(w_t)$, for some compression operator \mathcal{C}_w . The clients can then compute an unbiased gradient estimator at \hat{w}_t and send it back to the PS for aggregation.

While this method is fairly simple, it has inherent disadvantages. First, there is no enlarged time window during which clients can download the compressed model weights, as they can only do so at their participation round. Second, unlike with gradient compression, convergence in this setting can be guaranteed only to a proximity that is proportional to the compression error, rendering standard low-bit compression schemes unusable. Indeed, this is the case even for strongly convex functions, as shown by [Chraibi et al. \(2019\)](#) and reinforced by our counter-example in [Appendix A](#).

To tackle these challenges, our approach relies on the following relation: for any $\tau \geq 0$, we can decompose w_t into two ingredients: *Anchor* and *Correction*. Formally,

$$w_t = \underbrace{w_{t-\tau}}_{(i) \text{ Anchor}} + \underbrace{w_t - w_{t-\tau}}_{(ii) \text{ Correction}} .$$

This implies that:

- (i) If a client is notified at round $t - \tau$ about its participation at round t , it can start downloading the anchor, that is, $w_{t-\tau}$, *ahead of its participation round*,¹
- (ii) and thus, at round t , the client only needs to download the correction, that is, $w_t - w_{t-\tau}$.

Yet, merely relying on this relation is not sufficient to achieve our goals; additionally, we seek to *compress* both (i) and (ii). However, these terms are inherently different and therefore, should not be treated in the same manner. Essentially, the client has more time to download (i), which is the main ingredient that forms the model weights. Introducing a large error in this term may prevent the model from converging. Conversely, (ii) must be downloaded at the participation round of the client, but it is just the sum of τ recent gradients.

For (i), we develop a new compression technique (see §4), that achieves a better accuracy-bandwidth tradeoff than gradient compression techniques at the cost of higher complexity; we amortize its complexity over several rounds. Using this technique with only several bits per coordinate (e.g., 4) results in a negligible error. For (ii), we use standard gradient compression techniques with as low as 1 bit per coordinate. Since (ii) is only a sum of τ recent gradients, this error is expected to decay as training progresses.

Overall, we achieve both goals as (1) the download time window is enlarged, with only a small bandwidth fraction that must be used online; and (2) the total downlink bandwidth

¹In practice, the client can start downloading $w_{t-\tau}$ at round $t - \tau$ or $w_{t-\tau'}$ at round $t - \tau'$ for some $\tau' < \tau$, as long as the download is complete *before* round t .

Algorithm 1 DoCoFL – Parameter Server

Input: Initial weights $w_0 \in \mathbb{R}^d$, learning rate η , weights (anchors) compression \mathcal{C}_w , correction compression \mathcal{C}_c , anchor compression rate K , compressed anchors queue $Q \leftarrow \emptyset$ with capacity \mathcal{V} , client participation process $\mathcal{P}(\cdot)$

for $t = 0, \dots, T - 1$ **do**

▷ **Anchor Deployment**

if $t \bmod K == 0$ **then**

 Compress anchor, $\mathcal{C}_w(w_t)$

$Q.\text{enqueue}(\mathcal{C}_w(w_t))$

▷ If Q is full, $Q.\text{dequeue}()$

end if

▷ **Client Participation Process**

$\mathcal{S}_t \leftarrow \mathcal{P}(t)$

▷ $|\mathcal{S}_t| = S$; see §3.2

▷ **Optimization**

for client $i \in \mathcal{S}_t$ in parallel **do**

 Send compressed correction, $\hat{\Delta}_t^i$

▷ See Algorithm 2

 Obtain compressed local gradient, $\mathcal{C}_g(\hat{g}_t^i)$

end for

Aggregate local gradients, $\hat{g}_t := \frac{1}{S} \sum_{i \in \mathcal{S}_t} \mathcal{C}_g(\hat{g}_t^i)$

Update weights, $w_{t+1} = w_t - \eta \hat{g}_t$

end for

Algorithm 2 DoCoFL – Client i

Input: Gradient compression \mathcal{C}_g

Notification round s (by process \mathcal{P}):

Obtain participation round t

▷ $i \in \mathcal{P}(t), s \leq t$

Obtain latest compressed anchor, $y_t^i \leftarrow Q.\text{top}()$

▷ Within time window $[s, t]$

Participation round t :

Obtain compressed correction, $\hat{\Delta}_t^i = \mathcal{C}_c(w_t - y_t^i)$

Construct current model estimate, $\hat{w}_t^i = y_t^i + \hat{\Delta}_t^i$

Compute local gradient, $\hat{g}_t^i = g_t^i(\hat{w}_t^i)$

Compress and send local gradient, $\mathcal{C}_g(\hat{g}_t^i)$, to PS

usage is reduced by up to an order of magnitude compared to existing solutions and without degrading model accuracy.

In Figure 1, we show a timeline that illustrates the training procedure of DoCoFL, as we now formally detail on the role of the PS and the clients in our framework.

Parameter Server. As detailed in Algorithm 1, our PS executes three separate processes throughout the training procedure. First, it performs ① ‘anchor deployment’ – once in every K rounds, it compresses the model weights and stores the compressed weights in a queue Q of length \mathcal{V} . Second, the PS employs a client participation process, which we elaborate on in

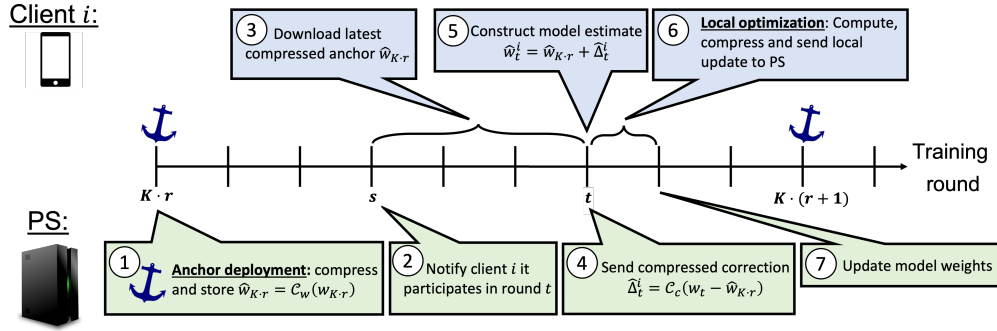


Figure 1: DoCoFL’s training procedure. Here, we illustrate the interaction between the PS and a single client. Typically, multiple clients participate in each training round, and each client may be notified about its participation in a different round.

§3.2; this process determines which clients will participate in a given round. Finally, in each round, the PS obtains the local model updates (i.e., gradients) from the clients participating in that round, computes their average, and ⑦ updates the model weights.

Client. Consider a client that is ② chosen by the PS at some round s to participate in some future round t . This means that in round $s \leq t$, the client is notified about its upcoming participation. It can then start ③ downloading the latest anchor stored by the PS; note that the client has a time window of length $t - s$ rounds to download the compressed anchor. At its participation round t , the client ④ obtains the compressed correction from the PS, i.e., the compressed difference between the updated model and the compressed anchor obtained earlier, to ⑤ construct an unbiased estimate of the updated model weights.² It then ⑥ locally computes a stochastic gradient, compresses it, and sends the compressed gradient to the PS; see Algorithm 2.

3.2 Client Participation Process

An important element in DoCoFL is the client participation process \mathcal{P} . For a round number t , it returns a subset of clients $\mathcal{S}_t \subseteq [N]$ of size S to participate in that round. Crucially, in DoCoFL, clients can be notified about their participation prior to their actual participation round.

This discrepancy between the notification and the participation round gives DoCoFL the desired versatility that opens the door for more clients to participate in the optimization process. While current frameworks follow a selection process that notifies a client about its participation just before it takes place, it is possible to consider useful selection/notification processes where some clients (e.g., with weaker connectivity) are notified earlier than others.

Another point to consider is the bias-utility tradeoff, where some choices of \mathcal{P} can allow more clients to participate but may introduce bias in the participation rounds of clients

²The client obtains the (unbiasedly) compressed difference between w_t and the *compressed* anchor rather than the exact anchor. This implies that the resulting model estimate is unbiased, even if the anchor compressor \mathcal{C}_w is biased. A similar error-compensation mechanism was previously used for gradient compression (i.e., ‘induced compressor’, Horváth and Richtárik (2020)).

with an untractable effect on the optimization process. Instead, we focus on processes that preserve the property where at each round, the PS obtains an unbiased estimate of the gradient, which means that we require \mathcal{P} to satisfy the following property: all clients have the same probability of participating in any given round t , i.e., $\mathbb{P}(i \in \mathcal{P}(t)) = S/N$. Surprisingly, such a restriction allows for a wide range of useful selection policies.

For example, consider a simple scenario where the PS has predetermined time windows T_s and T_w that it associates with “strongly connected” and “weakly connected” devices, respectively. Then, at each round t , the PS randomly selects clients but assigns their participation rounds to $t + T_s$ or $t + T_w$ according to their strength. Observe that this simple, yet very useful scenario satisfies the property we seek after T_w rounds (the first T_w rounds may take longer since, during these initial rounds, the weakly connected clients cannot be notified enough rounds prior to their participation).

3.3 Theoretical Guarantee

The primary challenge in analyzing downlink compression schemes for cross-device FL is that, even when using an unbiased compression method, i.e., that ensures $\mathbb{E}[\mathcal{C}_w(w_t)] = w_t$, the resulting gradient estimate $\nabla f(\mathcal{C}_w(w_t))$ may be biased. This is because, in general, the gradient is not a linear mapping. As mentioned, the resulting bias can hinder convergence, as illustrated in Appendix A, where we show that, gradient descent with weights compression do not reach the optimal solution even for strongly convex functions.

Accordingly, in this section, we show that DoCoFL converges to a stationary point when \mathcal{C}_w is the identity mapping, i.e., $\mathcal{C}_w(w) = w, \forall w \in \mathbb{R}^d$ – a setup that achieves our first goal (i.e., enlarged time window). As our analysis suggests, this identity assumption enables us to effectively bound the gradient bias resulting from the compression. For simplicity, we also assume no uplink compression (i.e., \mathcal{C}_g is also the identity function), although including it in our analysis is straightforward, and we do incorporate it in our experiments.

Following this result, and the result of [Chraibi et al. \(2019\)](#) in the convex case, in Appendix B, we give a theoretical intuition and empirical evidence for why DoCoFL works well in setups of interest when \mathcal{C}_w is *not* the identity function – achieving our second goal (i.e., total bandwidth reduction in the downlink direction).

Before we state our convergence result, we require an additional standard assumption about the correction compression operator \mathcal{C}_c , namely, that it has a bounded Normalized Mean-Squared-Error (NMSE) ([Philippenko and Dieuleveut, 2020](#); [Richtárik et al., 2021](#); [Vargaftik et al., 2021](#)).

Assumption 3.3. There exists an $\omega \in \mathbb{R}_+$ such that

$$\mathbb{E} [\|\mathcal{C}_c(w) - w\|^2] \leq \omega^2 \|w\|^2, \quad \forall w \in \mathbb{R}^d. \quad (4)$$

Equipped with the assumptions, we now give a convergence result for DoCoFL, namely, Theorem 3.4. Its full proof is deferred to Appendix C; here, we discuss the result and give a proof sketch.

Theorem 3.4. Let $\tilde{\sigma}^2 := \sigma^2 + 4\left(1 - \frac{S}{N}\right)G^2$, $\gamma := 1 + \left(1 - \frac{S}{N}\right)\frac{B^2}{S}$, and $M := f(w_0) - f^*$. Then, running DoCoFL with \mathcal{C}_w and \mathcal{C}_g as the identity mappings (and with appropriately selected η) guarantees

$$\mathbb{E} \left[\frac{1}{T} \sum_{t=0}^{T-1} \|\nabla f(w_t)\|^2 \right] \in \mathcal{O} \left(\sqrt{\frac{M\beta\tilde{\sigma}^2}{TS}} + \frac{(M^2\beta^2\omega^2K\mathcal{V}\tilde{\sigma}^2)^{1/3}}{T^{2/3}S^{1/3}} + \frac{\gamma M\beta(\omega K\mathcal{V} + 1)}{T} \right).$$

The convergence rate in Theorem 3.4 consists of three terms:

- The first term $\sqrt{\frac{M\beta\tilde{\sigma}^2}{TS}}$ is a slow statistical term that depends only on the noise level $\tilde{\sigma}^2$ (and the objective's properties); importantly, it is independent of DoCoFL's hyperparameters, K , \mathcal{V} , and ω .
- The last term $\frac{\gamma M\beta(\omega K\mathcal{V} + 1)}{T}$ is a fast deterministic term. When $\omega K\mathcal{V} \in \mathcal{O}(1)$ it decreases proportionally to $1/T$, and otherwise, it is proportional to $\omega K\mathcal{V}/T$.
- The middle term $\frac{(M^2\beta^2\omega^2K\mathcal{V}\tilde{\sigma}^2)^{1/3}}{T^{2/3}S^{1/3}}$ is a moderate term that depends on both noise level and DoCoFL's hyperparameters through the multiplication $\omega^2 K\mathcal{V}\tilde{\sigma}^2$; it is proportionate to $(T^{2/3}S^{1/3})^{-1}$.

Next, we derive observations from Theorem 3.4. For the ease of presentation, henceforth, we omit from $\mathcal{O}(\cdot)$ the dependence on M , β , and γ .

Corollary 3.5. When \mathcal{C}_c is the identity mapping, i.e., $\omega = 0$, clients obtain the exact model, and thus our method is equivalent to **FedAvg**. Indeed, we get the same asymptotic rate as **FedAvg** (McMahan et al., 2017; Karimireddy et al., 2019), namely, $\mathcal{O}(\sqrt{\tilde{\sigma}^2/TS} + 1/T)$.

Corollary 3.6. Typically, we are interested in the regime where $\omega K\mathcal{V} \in \Theta(1)$. In that case, we get the following asymptotic rate:

$$\mathcal{O} \left(\sqrt{\frac{\tilde{\sigma}^2}{TS}} + \frac{(\omega\tilde{\sigma}^2)^{1/3}}{T^{2/3}S^{1/3}} + \frac{1}{T} \right).$$

Comparing this rate with Corollary 3.5, we note that the middle term is the additional cost incurred for utilizing compression. Importantly, it decreases when we improve the correction compression, i.e., reduce ω .

Corollary 3.7. Consider $\omega = \Theta(1)$. Then, for $K\mathcal{V} \in \mathcal{O}(\sqrt{\tilde{\sigma}^2 T/S})$, the slow term dominates the rate, which is $\mathcal{O}(\sqrt{\tilde{\sigma}^2/TS})$; that is, we can set $K\mathcal{V}$ as large as $\mathcal{O}(\sqrt{\tilde{\sigma}^2 T/S})$ and still get, similarly to **FedAvg**, a speed-up with S , the number of participating clients per-round.

Proof Sketch. Denote: $\nabla_t := \nabla f(w_t)$ and $\hat{\nabla}_t := \mathbb{E}[\hat{g}_t]$. By the update rule, the smoothness of the objective and standard arguments, we obtain that

$$\mathbb{E}[f(w_{t+1}) - f(w_t)] \leq -\frac{\eta}{2}\mathbb{E}\|\nabla_t\|^2 + \frac{\beta\eta^2}{2}\mathbb{E}\|\hat{g}_t\|^2 + \frac{\eta}{2}\mathbb{E}\|\hat{\nabla}_t - \nabla_t\|^2. \quad (5)$$

Using the smoothness of f , we can bound the last term in the right-hand side, corresponding to the gradient bias, by the clients' average compression error:

$$\mathbb{E}\|\hat{\nabla}_t - \nabla_t\|^2 \leq \beta^2 \cdot \mathbb{E} \left[\frac{1}{S} \sum_{i \in \mathcal{S}_t} \|\hat{w}_t^i - w_t\|^2 \right]. \quad (6)$$

Additionally, in Lemma C.1, we derive the following bound on the second moment of the stochastic aggregated gradient:

$$\mathbb{E}\|\hat{g}_t\|^2 \leq \frac{\tilde{\sigma}^2}{S} + 4\gamma\mathbb{E}\|\nabla_t\|^2 + \frac{2\beta^2}{S} \mathbb{E} \left[\sum_{i \in \mathcal{S}_t} \|\hat{w}_t^i - w_t\|^2 \right]. \quad (7)$$

Plugging these bounds back to Eq. (5), we obtain:

$$\mathbb{E}[f(w_{t+1}) - f(w_t)] \leq \left(-\frac{\eta}{2} + 2\gamma\beta\eta^2\right) \mathbb{E}\|\nabla_t\|^2 + \frac{\beta\eta^2\tilde{\sigma}^2}{2S} + \left(\frac{\beta^2\eta}{2} + \beta^3\eta^2\right) \mathbb{E} \left[\frac{1}{S} \sum_{i \in \mathcal{S}_t} \|\hat{w}_t^i - w_t\|^2 \right]. \quad (8)$$

Recall that each client constructs the current model estimate by summing an anchor and a compressed correction, i.e., $\hat{w}_t^i = y_t^i + \mathcal{C}_c(w_t - y_t^i)$, where y_t^i (i.e., the anchor) is some model from up to $K\mathcal{V}$ rounds ago; for simplicity, assume that all clients obtain the oldest anchor, i.e., $y_t^i = w_{t-K\mathcal{V}}$. Therefore, using Assumption 3.3, we can bound the compression error by the difference between the current model and the obtained anchor, which is proportional to the sum of the last few (aggregated) gradients:

$$\mathbb{E}\|\hat{w}_t^i - w_t\|^2 \leq \omega^2 \mathbb{E}\|w_t - y_t^i\|^2 = \omega^2 \eta^2 \mathbb{E} \left\| \sum_{k=t-K\mathcal{V}}^{t-1} \hat{g}_k \right\|^2.$$

Decomposing each gradient into bias and variance as $\hat{g}_k = \hat{\nabla}_k + \hat{\xi}_k$, where $\mathbb{E}[\hat{\xi}_k] = 0$, we get:

$$\begin{aligned} \mathbb{E}\|\hat{w}_t^i - w_t\|^2 &\leq 2\omega^2 \eta^2 \mathbb{E} \left\| \sum_{k=t-K\mathcal{V}}^{t-1} \hat{\nabla}_k \right\|^2 + 2\omega^2 \eta^2 \mathbb{E} \left\| \sum_{k=t-K\mathcal{V}}^{t-1} \hat{\xi}_k \right\|^2 \\ &\leq 2\omega^2 \eta^2 K\mathcal{V} \sum_{k=t-K\mathcal{V}}^{t-1} \mathbb{E}\|\hat{\nabla}_k\|^2 + 2\omega^2 \eta^2 \sum_{k=t-K\mathcal{V}}^{t-1} \mathbb{E}\|\hat{\xi}_k\|^2, \end{aligned}$$

where we used the orthogonality of the noises, i.e., $\mathbb{E}[\hat{\xi}_k^\top \hat{\xi}_\ell] = 0$ for $k \neq \ell$. Plugging-in $\hat{\xi}_k = \hat{g}_k - \hat{\nabla}_k$, we obtain:

$$\mathbb{E}\|\hat{w}_t^i - w_t\|^2 \leq 6\omega^2 \eta^2 K\mathcal{V} \sum_{k=t-K\mathcal{V}}^{t-1} \mathbb{E}\|\hat{\nabla}_k\|^2 + 4\omega^2 \eta^2 \sum_{k=t-K\mathcal{V}}^{t-1} \mathbb{E}\|\hat{g}_k\|^2.$$

Using Eq. (6) and (7) to bound $\mathbb{E}\|\hat{\nabla}_k\|^2$ and $\mathbb{E}\|\hat{g}_k\|^2$, respectively, we get a recursive relation as the client compression error at round t depends on all prior errors. This is due to error

accumulation from computing the aggregated gradients at inaccurate iterates. Lemma C.2 provides a (non-recursive) bound on the compression error at round t . Plugging this bound back to Eq. (8), summing over $t = 0, \dots, T - 1$, and using some more algebra, we get:

$$\mathbb{E}[f(w_T) - f(w_0)] \leq -\frac{\eta}{4} \sum_{t=0}^{T-1} \mathbb{E} \|\nabla_t\|^2 + \left(\frac{\beta\eta^2}{2} + 12\beta^2\omega^2 K\mathcal{V}\eta^3 \right) \frac{T\tilde{\sigma}^2}{S}.$$

Rearranging terms, dividing by T , and tuning η concludes the proof. \square

It is important to note that our framework may also introduce some opportunities for system-wise improvements that are not captured by standard analysis. For example, with a larger pool of clients that are able to participate in a training procedure, it may be easier and faster to reach the desired threshold of participants in each round. Also, it may offer access to more data overall with a different resulting model. How to capture and model such potential benefits in a way that is consistent with and useful in real deployments? Indeed, this is an interesting and significant challenge for future work that may yield new FL policies.

4 Anchor Compression

Compressing the anchors is an essential building block of DoCoFL for reducing the total downlink bandwidth. While many compression techniques exist, most techniques were designed for gradient compression. Although we can use many such methods in our framework, it is less desirable to use a gradient compression scheme for anchor compression since the compression error of the anchor has a larger impact on the resulting model accuracy than the correction error; recall that the model weights, unlike the correction, do not decay throughout training. Accordingly, we designed a compression technique for that purpose.

We first observe that this technique is considerably less restricted on the PS side (i.e., compression) than on the client’s side (i.e., decompression). On the PS side, we typically have more resources and time (a new anchor is deployed only every K rounds) to employ more complex calculations, where at the client side we seek speed and lighter computations.

Consequently, we devised a compression method called *Entropy-Constrained Uniform Quantization (ECUQ)*. The main idea behind this approach is to approximate Entropy-Constrained Quantization (ECQ), which is an optimal scheme among a large family of quantization techniques (Chou et al., 1989). Intuitively, given some vector, ECQ finds the best quantization values (i.e., those that minimize the mean squared error) such that after quantization and entropy encoding (e.g., Huffman coding, Huffman (1952)) of the resulting quantized vector, a given budget constraint is respected. However, this approach is slow, complex, and unstable (sensitive to hyperparameters), which renders it unsuitable for online compression of large vectors.

As we detail in Appendix D, ECUQ employs a binary search to efficiently find the maximal number of *uniformly spaced* quantization values (between the minimal and maximal values of the input vector), such that after entropy encoding, the entropy of the quantized vector

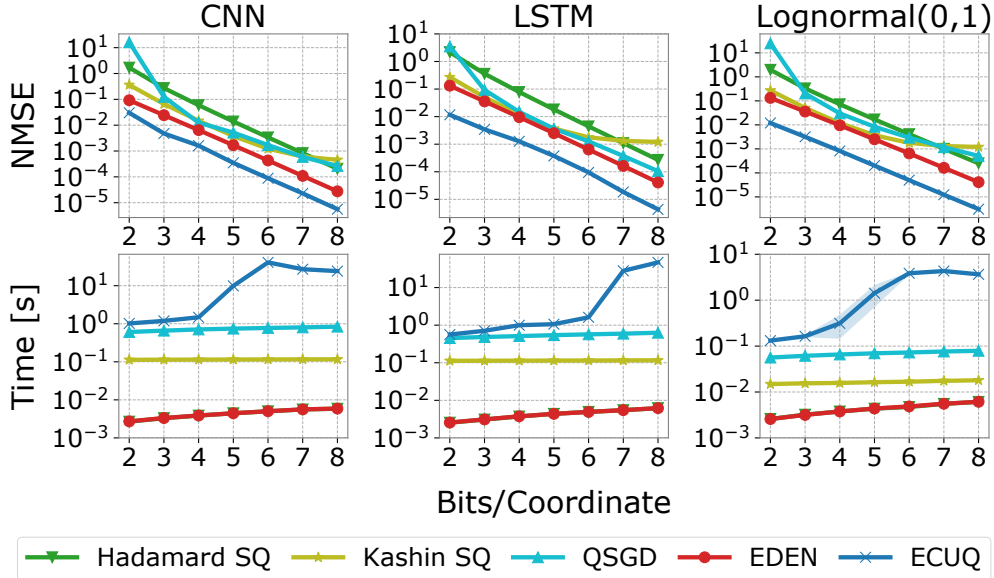


Figure 2: ECUQ vs. gradient compression methods: NMSE (**top**) and encoding time (**bottom**) for three different cases – recorded model parameters of a CNN (**left**); LSTM (**middle**); and vectors drawn from synthetic $LogNormal(0, 1)$ distribution (**right**).

would be within a small threshold from a given bandwidth constraint. Since computing the entropy of a vector does not require to actually encode it, the binary search is executed fast, and only after finding these quantization values, we encode the vector.

In Appendix D, we compare ECUQ, ECQ and a technique based on K-Means clustering (ECK-Means), which also approximates ECQ (see Figs. 6 and 7); our results indicate that ECUQ is always better than ECK-Means and competitive with ECQ while being orders of magnitude faster.

We also compare ECUQ with four recent gradient compression techniques: **(1)** Hadamard followed by stochastic quantization (SQ) (Suresh et al., 2017); **(2)** Kashin’s representation followed by SQ (Lyubarskii and Vershynin, 2010; Safaryan et al., 2022); **(3)** QSGD followed by Elias Gamma encoding (Alistarh et al., 2017); and **(4)** EDEN (Vargaftik et al., 2022). We test these in three different scenarios: **(1)** Model parameters of a convolutional neural network (CNN) with $\approx 11M$ parameters; **(2)** Model parameters of an LSTM network with $\approx 8M$ parameters; and **(3)** Synthetic vectors drawn from a $LogNormal(0, 1)$ distribution with 1M entries. We repeat each experiment ten times and report the mean.

As shown in Figure 2, ECUQ consistently offers the best NMSE, which is by up to an order of magnitude better than that of the second best. We also find that ECUQ is sufficiently fast to be used by the PS every several rounds (a typical cross-device FL round may take minutes to hours).

We note that a similar approach to ECUQ was used by Vargaftik et al. (2022) to determine *offline* near-optimal quantization values for the *normal distribution*; ECUQ, on the other hand, is applied *online* and to *any* input vector (and not a distribution).

5 Experiments

As previously mentioned, prior bi-directional/downlink compression methods rely on repeated client participation and are therefore incompatible with cross-device FL. Thus, to the best of our knowledge, DoCoFL is the first bandwidth reduction method for cross-device downlink compression. Accordingly, we compare its performance to that of an uncompressed baseline obtained by running FedAvg (McMahan et al., 2017) without any (i.e., uplink or downlink) compression, utilizing full precision (i.e., 32-bit floats) in both directions. Then, we perform an ablation study that shows the consistency of DoCoFL to its hyperparameters.

We cover a wide range of use cases that include two image classification and two language processing tasks with different configurations and data partitioning, as shortly summarized in Table 2 and further detailed in Appendix E.

Table 2: Tasks configuration.

Dataset	Net. (# params)	# clients (S)	Partition
CIFAR-100	ResNet-9 (4.9M)	200 (10)	I.I.D
EMNIST	LeNet (65K)	1000 (20)	Non-I.I.D
Amazon	LSTM (8.3M)	500 (10)	I.I.D
Shakespeare	LSTM (820K)	1129 (20)	Non-I.I.D

Image Classification. We use the CIFAR-100 and EMNIST datasets. For CIFAR-100 (Krizhevsky et al., 2009), the data distribution among the clients is i.i.d. For EMNIST (Cohen et al., 2017), the dataset of each client is composed of 10% i.i.d samples from the entire dataset and 90% i.i.d samples of 2 out of 47 classes (Karimireddy et al., 2020).

Language Processing. For language processing, we perform a sentiment analysis task on the Amazon Reviews dataset (Zhang et al., 2015) with i.i.d data partitioning; and a next-character prediction task on the Shakespeare dataset (McMahan et al., 2017), where each client holds data associated with a single role and play.

In all simulations, we run DoCoFL with ECUQ for anchor compression (i.e., \mathcal{C}_w), and EDEN (Vargaftik et al., 2022) for correction and uplink compression (i.e., \mathcal{C}_c and \mathcal{C}_g).

Main Results. In Table 3, we report the best validation accuracy achieved during training for FedAvg and two representative configurations of DoCoFL. It is evident that the validation accuracy of DoCoFL and FedAvg is always competitive. In some tasks, DoCoFL performs somewhat better. For example, for EMNIST, DoCoFL reduces the online downlink bandwidth by $16\times$ and the total by $8\times$ while achieving higher validation accuracy.

As is often the case in FL, our evaluation indicates that using more bandwidth does not necessarily lead to higher validation accuracy. While using less bandwidth usually impacts the train accuracy, as it implies a larger compression error, it may positively affect the model’s generalization ability. This is because it can act as a form of regularization, similar to adding noise to the input data. We further reinforce these observations in Appendix F, where we display validation and train accuracies as a function of the round number.

Table 3: Best validation accuracy for different tasks. The configuration triplet (b_w, b_c, b_g) means using $b_w, b_c,$ and b_g bits per coordinate for the anchor, correction, and gradient (uplink) compression, respectively. For all tasks, we use $K = 10$ and $\mathcal{V} = 3$.

		CIFAR-100		EMNIST		Amazon		Shakespeare	
		(b_w, b_c, b_g)	Accuracy	(b_w, b_c, b_g)	Accuracy	(b_w, b_c, b_g)	Accuracy	(b_w, b_c, b_g)	Accuracy
FedAvg		–	65.03	–	85.85	–	92.59	–	46.10
DoCoFL	Config 1	(2, 2, 1)	64.94	(4, 4, 3)	85.94	(6, 6, 2)	92.51	(4, 4, 4)	45.86
	Config 2	(2, 1/2, 1)	65.81	(2, 2, 3)	86.83	(4, 4, 2)	92.24	(2, 2, 4)	46.55

Ablation Study. Next, we evaluate the effect of the hyperparameters K and \mathcal{V} on DoCoFL’s performance. In Fig. 3, we report the final *train* accuracy of DoCoFL for the CIFAR-100 task with varying values of $K \in \{10, 50, 100, 500\}$ and $\mathcal{V} \in \{3, 5, 10\}$ under two bandwidth configurations. The results indicate that our framework performs as expected for a wide range of anchor deployment rates and queue capacities. As we elaborate in Appendix F and in line with our theoretical findings, the norm of the correction becomes sizable when $K\mathcal{V}$ is too large, which can hinder the final accuracy and even convergence. To allow the usage of large $K\mathcal{V}$, one may increase the correction bandwidth, trading online bandwidth for a larger anchor download time window.

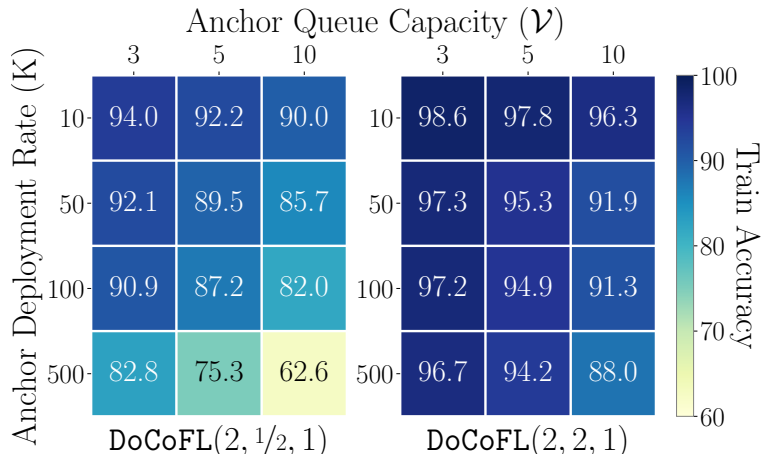


Figure 3: Final train accuracy of DoCoFL for two bandwidth configurations and various values of K and \mathcal{V} on the CIFAR-100 task.

6 Conclusion

In this work, we presented DoCoFL, a framework for downlink compression in the challenging cross-device FL setup. By enlarging the clients’ model download time window, reducing total downlink bandwidth requirements, and allowing for uplink compression, DoCoFL is designed to allow more resource-constrained and diverse clients to participate in the training procedure. Experiments over various tasks indicate that DoCoFL indeed significantly reduces bi-directional bandwidth usage while performing competitively with an uncompressed baseline.

As future work, we propose to study how to combine DoCoFL with the delayed gradients framework (Stich and Karimireddy, 2019). While delayed gradients do not reduce downlink bandwidth, they are especially useful for clients that may require a long time to perform local updates and communicate them back to the PS. Thus, accounting for delayed gradients may improve DoCoFL’s versatility and robustness in real FL deployments. Additionally, as we convey in Appendix B, one may consider extending DoCoFL to use adaptive bandwidth budget for anchor and correction compression; although it introduces a significant theoretical challenge due to the coupling between optimization and compression, it has the potential to yield a convergence guarantee for DoCoFL with anchor compression and achieve even larger bandwidth savings.

Acknowledgements

Kfir Y. Levy is supported in part by the Israel Science Foundation (grant No. 447/20).

References

- D. Alistarh, D. Grubic, J. Li, R. Tomioka, and M. Vojnovic. QSGD: Communication-efficient SGD via gradient quantization and encoding. *Advances in neural information processing systems*, 30, 2017.
- D. Alistarh, T. Hoeffler, M. Johansson, N. Konstantinov, S. Khirirat, and C. Renggli. The convergence of sparsified gradient methods. *Advances in Neural Information Processing Systems*, 31, 2018.
- J. Bernstein, Y.-X. Wang, K. Azizzadenesheli, and A. Anandkumar. signSGD: Compressed optimisation for non-convex problems. In *International Conference on Machine Learning*, pages 560–569. PMLR, 2018a.
- J. Bernstein, J. Zhao, K. Azizzadenesheli, and A. Anandkumar. signSGD with majority vote is communication efficient and fault tolerant. *arXiv preprint arXiv:1810.05291*, 2018b.
- P. A. Chou, T. Lookabaugh, and R. M. Gray. Entropy-constrained vector quantization. *IEEE Transactions on acoustics, speech, and signal processing*, 37(1):31–42, 1989.
- S. Chraïbi, A. Khaled, D. Kovalev, P. Richtárik, A. Salim, and M. Takáč. Distributed fixed point methods with compressed iterates. *arXiv preprint arXiv:1912.09925*, 2019.
- G. Cohen, S. Afshar, J. Tapson, and A. Van Schaik. EMNIST: Extending MNIST to hand-written letters. In *2017 international joint conference on neural networks (IJCNN)*, pages 2921–2926. IEEE, 2017.

- E. Gorbunov, K. P. Burlachenko, Z. Li, and P. Richtárik. MARINA: Faster non-convex distributed learning with compression. In *International Conference on Machine Learning*, pages 3788–3798. PMLR, 2021.
- K. Gruntkowska, A. Tyurin, and P. Richtárik. EF21-P and Friends: Improved Theoretical Communication Complexity for Distributed Optimization with Bidirectional Compression. *arXiv preprint arXiv:2209.15218*, 2022.
- S. Horváth and P. Richtárik. A better alternative to error feedback for communication-efficient distributed learning. *arXiv preprint arXiv:2006.11077*, 2020.
- D. Howdle. Worldwide mobile data pricing. <https://www.cable.co.uk/mobiles/worldwide-data-pricing/#pricing>, 2022.
- D. A. Huffman. A method for the construction of minimum-redundancy codes. *Proceedings of the IRE*, 40(9):1098–1101, 1952.
- N. Iykin, D. Rothchild, E. Ullah, I. Stoica, R. Arora, et al. Communication-efficient distributed SGD with sketching. *Advances in Neural Information Processing Systems*, 32, 2019.
- R. Jin, Y. Huang, X. He, H. Dai, and T. Wu. Stochastic-sign SGD for federated learning with theoretical guarantees. *arXiv preprint arXiv:2002.10940*, 2020.
- P. Kairouz, H. B. McMahan, B. Avent, A. Bellet, M. Bennis, A. N. Bhagoji, K. Bonawitz, Z. Charles, G. Cormode, R. Cummings, et al. Advances and open problems in federated learning. *Foundations and Trends® in Machine Learning*, 14(1–2):1–210, 2021.
- S. P. Karimireddy, Q. Rebjock, S. Stich, and M. Jaggi. Error feedback fixes signsgd and other gradient compression schemes. In *International Conference on Machine Learning*, pages 3252–3261. PMLR, 2019.
- S. P. Karimireddy, S. Kale, M. Mohri, S. Reddi, S. Stich, and A. T. Suresh. Scaffold: Stochastic controlled averaging for federated learning. In *International Conference on Machine Learning*, pages 5132–5143. PMLR, 2020.
- A. Koloskova, N. Loizou, S. Boreiri, M. Jaggi, and S. Stich. A unified theory of decentralized sgd with changing topology and local updates. In *International Conference on Machine Learning*, pages 5381–5393. PMLR, 2020.
- J. Konečný and P. Richtárik. Randomized distributed mean estimation: Accuracy vs. communication. *Frontiers in Applied Mathematics and Statistics*, 4:62, 2018.
- J. Konečný, H. B. McMahan, D. Ramage, and P. Richtárik. Federated optimization: Distributed machine learning for on-device intelligence. *arXiv preprint arXiv:1610.02527*, 2016a.

- J. Konečný, H. B. McMahan, F. X. Yu, P. Richtárik, A. T. Suresh, and D. Bacon. Federated learning: Strategies for improving communication efficiency. *arXiv preprint arXiv:1610.05492*, 2016b.
- A. Krizhevsky, G. Hinton, et al. Learning multiple layers of features from tiny images. 2009.
- X. Liu, Y. Li, J. Tang, and M. Yan. A double residual compression algorithm for efficient distributed learning. In *International Conference on Artificial Intelligence and Statistics*, pages 133–143. PMLR, 2020.
- Y. Lyubarskii and R. Vershynin. Uncertainty principles and vector quantization. *IEEE Transactions on Information Theory*, 56(7):3491–3501, 2010.
- B. McMahan and D. Ramage. Federated learning: Collaborative machine learning without centralized training data. <https://ai.googleblog.com/2017/04/federated-learning-collaborative.html>, 2017.
- B. McMahan, E. Moore, D. Ramage, S. Hampson, and B. A. y Arcas. Communication-efficient learning of deep networks from decentralized data. In *Artificial intelligence and statistics*, pages 1273–1282. PMLR, 2017.
- H. B. McMahan, A. Thakurta, G. Andrew, B. Balle, P. Kairouz, D. Ramage, S. Song, T. Steinke, A. Terzis, O. Thakkar, et al. Federated learning with formal differential privacy guarantees. *Google AI Blog*, 2022.
- D. Ng, X. Lan, M. M.-S. Yao, W. P. Chan, and M. Feng. Federated learning: a collaborative effort to achieve better medical imaging models for individual sites that have small labelled datasets. *Quantitative Imaging in Medicine and Surgery*, 11(2):852, 2021.
- A. Paszke, S. Gross, F. Massa, A. Lerer, J. Bradbury, G. Chanan, T. Killeen, Z. Lin, N. Gimeshein, L. Antiga, et al. Pytorch: An imperative style, high-performance deep learning library. *Advances in neural information processing systems*, 32, 2019.
- C. Philippenko and A. Dieuleveut. Bidirectional compression in heterogeneous settings for distributed or federated learning with partial participation: tight convergence guarantees. *arXiv preprint arXiv:2006.14591*, 2020.
- C. Philippenko and A. Dieuleveut. Preserved central model for faster bidirectional compression in distributed settings. *Advances in Neural Information Processing Systems*, 34: 2387–2399, 2021.
- A. Ramezani-Kebrya, F. Faghri, I. Markov, V. Aksenov, D. Alistarh, and D. M. Roy. NUQSGD: Provably Communication-efficient Data-parallel SGD via Nonuniform Quantization. *J. Mach. Learn. Res.*, 22:114–1, 2021.

- P. Richtárik, I. Sokolov, and I. Fatkhullin. EF21: A new, simpler, theoretically better, and practically faster error feedback. *Advances in Neural Information Processing Systems*, 34: 4384–4396, 2021.
- D. Rothchild, A. Panda, E. Ullah, N. Ivkin, I. Stoica, V. Braverman, J. Gonzalez, and R. Arora. FetchSGD: Communication-efficient federated learning with sketching. In *International Conference on Machine Learning*, pages 8253–8265. PMLR, 2020.
- M. Safaryan, E. Shulgin, and P. Richtárik. Uncertainty principle for communication compression in distributed and federated learning and the search for an optimal compressor. *Information and Inference: A Journal of the IMA*, 11(2):557–580, 2022.
- F. Seide, H. Fu, J. Droppo, G. Li, and D. Yu. 1-bit stochastic gradient descent and its application to data-parallel distributed training of speech dnns. In *Fifteenth annual conference of the international speech communication association*, 2014.
- N. Shlezinger, M. Chen, Y. C. Eldar, H. V. Poor, and S. Cui. UVeQFed: Universal vector quantization for federated learning. *IEEE Transactions on Signal Processing*, 69:500–514, 2020.
- J. Stewart. *Calculus*. Cengage Learning, 2015.
- S. U. Stich and S. P. Karimireddy. The error-feedback framework: Better rates for SGD with delayed gradients and compressed communication. *arXiv preprint arXiv:1909.05350*, 2019.
- H. Sumra. Best and Worst Countries for Wi-Fi Access. <https://www.ooma.com/blog/best-worst-wifi-countries/>, July 2020.
- A. T. Suresh, X. Y. Felix, S. Kumar, and H. B. McMahan. Distributed mean estimation with limited communication. In *International conference on machine learning*, pages 3329–3337. PMLR, 2017.
- H. Tang, C. Yu, X. Lian, T. Zhang, and J. Liu. Doublesqueeze: Parallel stochastic gradient descent with double-pass error-compensated compression. In *International Conference on Machine Learning*, pages 6155–6165. PMLR, 2019.
- S. Vargaftik, R. Ben-Basat, A. Portnoy, G. Mendelson, Y. Ben-Itzhak, and M. Mitzenmacher. DRIVE: one-bit distributed mean estimation. *Advances in Neural Information Processing Systems*, 34:362–377, 2021.
- S. Vargaftik, R. B. Basat, A. Portnoy, G. Mendelson, Y. B. Itzhak, and M. Mitzenmacher. EDEN: Communication-efficient and robust distributed mean estimation for federated learning. In *International Conference on Machine Learning*, pages 21984–22014. PMLR, 2022.

- T. Vogels, S. P. Karimireddy, and M. Jaggi. PowerSGD: Practical low-rank gradient compression for distributed optimization. *Advances in Neural Information Processing Systems*, 32, 2019.
- J. Wang, Q. Liu, H. Liang, G. Joshi, and H. V. Poor. Tackling the objective inconsistency problem in heterogeneous federated optimization. *Advances in neural information processing systems*, 33:7611–7623, 2020.
- W. Wen, C. Xu, F. Yan, C. Wu, Y. Wang, Y. Chen, and H. Li. Terngrad: Ternary gradients to reduce communication in distributed deep learning. *Advances in neural information processing systems*, 30, 2017.
- W. Yang, Y. Zhang, K. Ye, L. Li, and C.-Z. Xu. FFD: A federated learning based method for credit card fraud detection. In *International conference on big data*, pages 18–32. Springer, 2019.
- X. Zhang, J. Zhao, and Y. LeCun. Character-level convolutional networks for text classification. *Advances in neural information processing systems*, 28, 2015.
- S. Zheng, Z. Huang, and J. Kwok. Communication-efficient distributed blockwise momentum SGD with error-feedback. *Advances in Neural Information Processing Systems*, 32, 2019.

A Gradient Descent with Weights Compression is Suboptimal

In this section, we give an example of a (strongly) convex function on \mathbb{R} , for which we show that running gradient descent with gradients computed at estimated (i.e., lossily compressed and then decompressed) iterates (rather than at the iterates themselves) does not converge to the global minimum. Instead, it converges to a suboptimal solution.

Let $f : \mathbb{R} \rightarrow \mathbb{R}$ be the following convex and smooth function:

$$f(w) = \frac{1}{2}(w - 1)^2 + \frac{1}{2}[w - 1]_+^2 ,$$

where $[w]_+ = \max(0, w)$. Note that $w^* = 1$ is the global minimizer of f . We analyze the following update rule:

$$\begin{aligned} w_{t+1} &= w_t - \eta \nabla f(\hat{w}_t) \\ \hat{w}_t &= \mathcal{C}_w(w_t) , \end{aligned}$$

where $\eta > 0$ is the step size, and $\mathcal{C} : \mathbb{R} \rightarrow \mathbb{R}$ is a randomized, unbiased compression operator with bounded NMSE, i.e.,

$$\mathbb{E}[\mathcal{C}_w(w)] = w, \quad \mathbb{E}|\mathcal{C}_w(w) - w|^2 \leq \omega_w^2 |w|^2, \quad \forall w \in \mathbb{R} .$$

We can alternatively write: $\hat{w}_t = w_t + \epsilon_t |w_t|$, where $\mathbb{E}[\epsilon_t] = 0$, $\mathbb{E}[\epsilon_t^2] \leq \omega_w^2$, and $\{\epsilon_t\}_t$ are independent. Thus, we can rewrite the above update rule as

$$w_{t+1} = w_t - \eta \nabla f(w_t + \epsilon_t |w_t|) . \tag{9}$$

In Eq. (9), we repeatedly apply the stochastic mapping: $w \mapsto w - \eta \nabla f(w + \epsilon |w|)$. If this process converges in expectation, it converges to a point \tilde{w} for which $\mathbb{E}[\nabla f(\tilde{w} + \epsilon |\tilde{w}|)] = 0$. We show that $w^* = 1$ does not satisfy this condition, which will imply that this process does not converge to w^* . First, note that f is differentiable, and $\nabla f(w) = (w - 1) + [w - 1]_+$. Thus,

$$\mathbb{E}[\nabla f(w^* + \epsilon |w^*|)] = \mathbb{E}[\nabla f(1 + \epsilon)] = \mathbb{E}[\epsilon + [\epsilon]_+] = \mathbb{E}[\epsilon]_+ ,$$

where the last equality follows from the linearity of expectation, $\mathbb{E}[\epsilon] = 0$. Now, note that unless $\epsilon = 0$ almost surely, we necessarily have $\mathbb{E}[\max\{0, \epsilon\}] > 0$, which implies that the iterative update in Eq. (9) does not converge in expectation to $w^* = 1$.

B Why DoCoFL with Anchor Compression Works

To support Theorem 3.4, in which we establish the convergence of DoCoFL when the anchor compression \mathcal{C}_w is identity, in this section, we give theoretical intuition and numerical results to support it for why DoCoFL also works when \mathcal{C}_w is not the identity mapping.

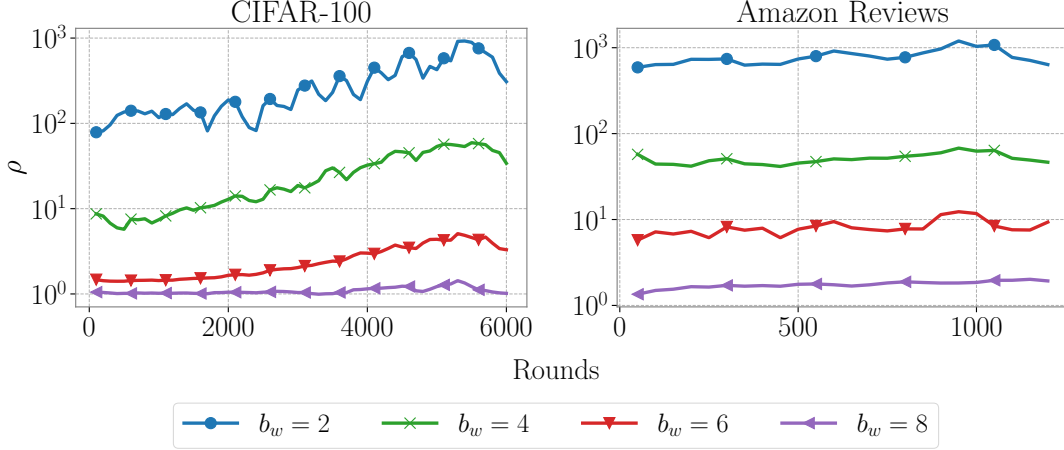


Figure 4: Client estimation error ratio ρ_t on the CIFAR-100 and Amazon Reviews tasks for different anchor compression budgets. For both tasks, we used 2 bits per coordinate for the correction and gradients (uplink) compression.

Consider the framework we analyze in Appendix C, namely the generalization of DoCoFL given by Algorithm 3. Adding an anchor compressor (i.e., \mathcal{C}_w) implies that each client now obtains a **compressed** outdated model $\hat{y}_t^i = \mathcal{C}_w(y_t^i)$ and a corresponding correction $\hat{\Delta}_t^i = \mathcal{C}_c(w_t - \hat{y}_t^i)$, and constructs $\hat{w}_t^i = \hat{y}_t^i + \hat{\Delta}_t^i$. Thus, adding an anchor compression affects the client’s model estimation error $\mathbb{E} \|\hat{w}_t^i - w_t\|^2$, which we bound in Eq. (23).

Denote by $e_{t,i}^2 := \|y_t^i + \hat{\Delta}_t^i - w_t\|^2$ the client’s squared estimation error when not using anchor compression (i.e., when \mathcal{C}_w is identity), and by $\hat{e}_{t,i}^2 := \|\hat{y}_t^i + \hat{\Delta}_t^i - w_t\|^2$ the squared estimation error when using anchor compression. If one could show that the following condition holds:

$$\mathbb{E}[\hat{e}_{t,i}^2] \leq C^2 \mathbb{E}[e_{t,i}^2], \quad (10)$$

for some moderate $C > 0$, then we can simply bound $\mathbb{E}[\hat{e}_{t,i}^2]$ in the left-hand side of Eq. (23), and the rest of our analysis holds. However, we know that, in general, this condition does not hold (recall the counterexample in Appendix A).

Nevertheless, we empirically show that it holds in our evaluation where we have non-convex and noisy optimization. More generally, in cross-device FL, client sampling and stochastic gradient estimation add natural noise to the optimization process, and we empirically show that the additional estimation error due to anchor compression with ECUQ is sufficiently low and allows convergence, as conveyed above.

In Fig. 4 we present the ratio $\rho_t := \sum_{i \in \mathcal{S}_t} \hat{e}_{t,i}^2 / \sum_{i \in \mathcal{S}_t} e_{t,i}^2$ for different anchor compression budgets in CIFAR-100 and Amazon Reviews experiments. First, note that the ratio is mostly stable throughout the entire training. Additionally, when we increase the bandwidth for anchor compression, the ratio decreases, to the extent that for 8 bits per coordinate, the ratio is ≈ 1 ; this is when the error induced by the correction compression dominates the estimation error.

We note that our intuition gives rise to using an adaptive budget for anchor compression; since ρ_t can be measured by the PS (i.e., it has access to y_t^i, \hat{y}_t^i, w_t and the correction

compressor \mathcal{C}_c), we can keep track of it, and increase the anchor compression budget if ρ_t is too large. We leave such investigation to future work.

C Proof of Theorem 3.4

In this section we prove Theorem 3.4, which we restate here for convenience,

Theorem 3.4. *Let $\tilde{\sigma}^2 := \sigma^2 + 4\left(1 - \frac{S}{N}\right)G^2$, $\gamma := 1 + \left(1 - \frac{S}{N}\right)\frac{B^2}{S}$, and $M := f(w_0) - f^*$. Then, running DoCoFL with \mathcal{C}_w and \mathcal{C}_g as the identity mappings (and with appropriately selected η) guarantees*

$$\mathbb{E} \left[\frac{1}{T} \sum_{t=0}^{T-1} \|\nabla f(w_t)\|^2 \right] \in \mathcal{O} \left(\sqrt{\frac{M\beta\tilde{\sigma}^2}{TS}} + \frac{(M^2\beta^2\omega^2K\mathcal{V}\tilde{\sigma}^2)^{1/3}}{T^{2/3}S^{1/3}} + \frac{\gamma M\beta(\omega K\mathcal{V} + 1)}{T} \right).$$

Proof. To simplify mathematical notations and computations, we analyze a more general framework than DoCoFL, where at each round, each client can download *any* model from up to \mathcal{T} rounds prior to their participation round as anchor. This generalized policy is described in Algorithm 3.

Algorithm 3 Meta-Algorithm (generalization of DoCoFL)

Input: Initial weights $w_0 \in \mathbb{R}^d$, learning rate η , correction compression \mathcal{C}_c , client participation process $\mathcal{P}(\cdot)$

for $t = 0, \dots, T - 1$ **do**

Obtain participating clients, $\mathcal{S}_t \leftarrow \mathcal{P}(t)$ $\triangleright |\mathcal{S}_t| = S$

for client $i \in \mathcal{S}_t$ in parallel **do**

Obtain model weights (anchor), $y_t^i = w_{t-\tau_t^i}$ $\triangleright \tau_t^i \in [0, \mathcal{T}]$

Obtain compressed correction, $\hat{\Delta}_t^i = \mathcal{C}_c(w_t - y_t^i)$

Construct model estimate, $\hat{w}_t^i = y_t^i + \hat{\Delta}_t^i$

Compute local gradient, $\hat{g}_t^i = g_t^i(\hat{w}_t^i)$

Communicate \hat{g}_t^i back to server

end for

Aggregate local gradients, $\hat{g}_t := \frac{1}{S} \sum_{i \in \mathcal{S}_t} \hat{g}_t^i$

Update weights, $w_{t+1} = w_t - \eta \hat{g}_t$

end for

Using Theorem 1, that proves the convergence of Algorithm 3 (see Appendix C.1), we prove Theorem 3.4. Namely, DoCoFL with \mathcal{C}_w and \mathcal{C}_g as identity mappings is a private case of Algorithm 3 where $\mathcal{T} = K\mathcal{V}$ and clients can only download models from specific prior rounds (multiplications of K). Thus, plugging-in $\mathcal{T} = K\mathcal{V}$ to Theorem 1 concludes the proof. \square

C.1 Proof of Theorem 1

Theorem 1. *Suppose Assumptions 3.1-3.3 are satisfied. Let $\tilde{\sigma}^2 := \sigma^2 + 4(1 - \frac{S}{N})G^2$, $\gamma := 1 + (1 - \frac{S}{N})\frac{B^2}{S}$, $\theta := \omega\mathcal{T} + 1$, and $M := f(w_0) - f^*$. Then, running Algorithm 3 with $\eta = \min \left\{ \frac{1}{30\gamma\beta\theta}, \sqrt{\frac{2MS}{\beta\tilde{\sigma}^2T}}, \left(\frac{MS}{12\beta^2\omega^2\mathcal{T}\tilde{\sigma}^2T}\right)^{1/3} \right\}$ guarantees*

$$\mathbb{E} \left[\frac{1}{T} \sum_{t=0}^{T-1} \|\nabla f(w_t)\|^2 \right] \leq 4\sqrt{\frac{2M\beta\tilde{\sigma}^2}{TS}} + 8\frac{(12M^2\beta^2\omega^2\mathcal{T}\tilde{\sigma}^2)^{1/3}}{T^{2/3}S^{1/3}} + \frac{120\gamma M\beta\theta}{T}. \quad (11)$$

Proof. For the ease of notation, let $\nabla_t := \nabla f(w_t)$ and $\tilde{\sigma}_S^2 := \tilde{\sigma}^2/S$. Throughout our analysis, we sometimes use \hat{w}_t^i even when $i \notin \mathcal{S}_t$, which is not well-defined. To resolve this, one can think about the following mathematically equivalent process, where at each round, all clients $i \in [N]$ obtain some previous model (anchor) y_t^i and the corresponding correction $\hat{\Delta}_t^i$, but only $i \in \mathcal{S}_t$ actually participate in the optimization. In that sense, for all $i \notin \mathcal{S}_t$, \hat{w}_t^i is the estimated model of client i if it were to participate in round t .

Let $\hat{\nabla}_t := \frac{1}{N} \sum_{i \in [N]} \nabla f_i(\hat{w}_t^i) = \mathbb{E}[\hat{g}_t]$. From the β -smoothness of the objective,

$$\begin{aligned} \mathbb{E}[f(w_{t+1}) - f(w_t)] &\leq -\eta\mathbb{E}[\hat{g}_t^\top \nabla_t] + \frac{\beta\eta^2}{2}\mathbb{E}\|\hat{g}_t\|^2 \\ &= -\eta\mathbb{E}[\hat{\nabla}_t^\top \nabla_t] + \frac{\beta\eta^2}{2}\mathbb{E}\|\hat{g}_t\|^2 \\ &= -\eta\mathbb{E}\|\nabla_t\|^2 + \underbrace{\eta\mathbb{E}[\nabla_t^\top (\nabla_t - \hat{\nabla}_t)]}_{=(A)} + \frac{\beta\eta^2}{2}\mathbb{E}\|\hat{g}_t\|^2, \end{aligned} \quad (12)$$

where the first equality follows from the law of total expectation, and the second equality from the linearity of expectation.

Bounding (A): Using the inequality $a^\top b \leq \frac{1}{2}\|a\|^2 + \frac{1}{2}\|b\|^2$, we get that

$$\eta\mathbb{E}[\nabla_t^\top (\nabla_t - \hat{\nabla}_t)] \leq \frac{\eta}{2}\mathbb{E}\|\nabla_t\|^2 + \frac{\eta}{2}\mathbb{E}\|\nabla_t - \hat{\nabla}_t\|^2.$$

Focusing on the second term in the right-hand side, we have:

$$\begin{aligned} \mathbb{E}\|\nabla_t - \hat{\nabla}_t\|^2 &= \mathbb{E} \left\| \frac{1}{N} \sum_{i=1}^N (\nabla f_i(w_t) - \nabla f_i(\hat{w}_t^i)) \right\|^2 \\ &\leq \frac{1}{N} \sum_{i=1}^N \mathbb{E} \|\nabla f_i(w_t) - \nabla f_i(\hat{w}_t^i)\|^2 \\ &\leq \frac{\beta^2}{N} \sum_{i=1}^N \mathbb{E} \|\hat{w}_t^i - w_t\|^2, \end{aligned} \quad (13)$$

where in the first inequality we used Lemma C.5, and the second inequality follows from the β -smoothness of each f_i . Plugging back this bound, we get:

$$\eta \mathbb{E}[\nabla_t^\top (\nabla_t - \hat{\nabla}_t)] \leq \frac{\eta}{2} \mathbb{E} \|\nabla_t\|^2 + \frac{\beta^2 \eta}{2N} \sum_{i=1}^N \mathbb{E} \|\hat{w}_t^i - w_t\|^2.$$

Using Lemma C.1 to bound $\mathbb{E} \|\hat{g}_t\|^2$ and the bound on (A), we get from Eq. (12) that

$$\begin{aligned} \mathbb{E}[f(w_{t+1}) - f(w_t)] &\leq -\frac{\eta}{2} \mathbb{E} \|\nabla_t\|^2 + \frac{\beta^2 \eta}{2N} \sum_{i=1}^N \mathbb{E} \|\hat{w}_t^i - w_t\|^2 \\ &\quad + \frac{\beta \eta^2}{2} \left(\tilde{\sigma}_S^2 + 4\gamma \mathbb{E} \|\nabla_t\|^2 + \frac{2\beta^2}{N} \sum_{i=1}^N \mathbb{E} \|\hat{w}_t^i - w_t\|^2 \right) \\ &= \left(-\frac{\eta}{2} + 2\gamma\beta\eta^2 \right) \mathbb{E} \|\nabla_t\|^2 + \frac{\beta\eta^2 \tilde{\sigma}_S^2}{2} \\ &\quad + \left(\frac{\beta^2 \eta}{2} + \beta^3 \eta^2 \right) \cdot \frac{1}{N} \sum_{i=1}^N \mathbb{E} \|\hat{w}_t^i - w_t\|^2. \end{aligned}$$

Applying Lemma C.2, we can bound $\frac{1}{N} \sum_{i=1}^N \mathbb{E} \|\hat{w}_t^i - w_t\|^2$ to get that

$$\begin{aligned} \mathbb{E}[f(w_{t+1}) - f(w_t)] &\leq \left(-\frac{\eta}{2} + 2\gamma\beta\eta^2 \right) \mathbb{E} \|\nabla_t\|^2 + \frac{\beta\eta^2 \tilde{\sigma}_S^2}{2} \\ &\quad + \left(\frac{\beta^2 \eta}{2} + \beta^3 \eta^2 \right) \left[\alpha \left(1 + \sum_{k=1}^t k(\rho\mathcal{T})^k \right) \tilde{\sigma}_S^2 + \frac{2\gamma}{\beta^2 \mathcal{T}} \sum_{k=1}^t (\rho\mathcal{T})^k \sum_{\ell=t-k\mathcal{T}}^{t-k} \mathbb{E} \|\nabla_\ell\|^2 \right] \\ &= \left(-\frac{\eta}{2} + 2\gamma\beta\eta^2 \right) \mathbb{E} \|\nabla_t\|^2 + \left[\frac{\beta\eta^2}{2} + \alpha \left(\frac{\beta^2 \eta}{2} + \beta^3 \eta^2 \right) \left(1 + \sum_{k=1}^t k(\rho\mathcal{T})^k \right) \right] \tilde{\sigma}_S^2 \\ &\quad + \underbrace{\left(\frac{\beta^2 \eta}{2} + \beta^3 \eta^2 \right) \frac{2\gamma}{\beta^2 \mathcal{T}} \sum_{k=1}^t (\rho\mathcal{T})^k \sum_{\ell=t-k\mathcal{T}}^{t-k} \mathbb{E} \|\nabla_\ell\|^2}_{=(B)}, \end{aligned} \tag{14}$$

where $\alpha = 4\omega^2 \eta^2 \mathcal{T}$ and $\rho = 20\beta^2 \omega^2 \eta^2 \mathcal{T}$. Since $\eta \leq \frac{1}{30\gamma\beta(\omega\mathcal{T}+1)} \leq \frac{1}{\sqrt{40}\beta\omega\mathcal{T}}$, it holds that $\rho\mathcal{T} = 20\beta^2 \omega^2 \mathcal{T}^2 \eta^2 \leq 1/2 < 1$, and thus we can bound the coefficient of $\tilde{\sigma}_S^2$ using Lemma C.7 as

$$\sum_{k=1}^t k(\rho\mathcal{T})^k \leq \sum_{k=1}^{\infty} k(\rho\mathcal{T})^k = \frac{\rho\mathcal{T}}{(1-\rho\mathcal{T})^2} \leq 4\rho\mathcal{T} \leq 2, \tag{15}$$

where we used $\frac{1}{(1-\rho\mathcal{T})^2} \leq 4$, and $\rho\mathcal{T} \leq 1/2$.

Bounding (B): To bound (B), we change the summation order. Consider a fixed $\ell \in \mathbb{N}$. Note that $(\rho\mathcal{T})^k$ appears as a coefficient of $\mathbb{E} \|\nabla_\ell\|^2$ if and only if $t - k\mathcal{T} \leq \ell \leq t - k$, which

is equivalent to $\frac{t-\ell}{\mathcal{T}} \leq k \leq t-\ell$. Therefore, we have

$$\begin{aligned} \sum_{k=1}^t (\rho\mathcal{T})^k \sum_{\ell=t-k\mathcal{T}}^{t-k} \mathbb{E} \|\nabla_\ell\|^2 &= \sum_{\ell=0}^{t-1} \left(\sum_{k=\lceil \frac{t-\ell}{\mathcal{T}} \rceil}^{t-\ell} (\rho\mathcal{T})^k \right) \mathbb{E} \|\nabla_\ell\|^2 \\ &\leq \sum_{\ell=0}^{t-1} \left(\sum_{k=\lceil \frac{t-\ell}{\mathcal{T}} \rceil}^{\infty} (\rho\mathcal{T})^k \right) \mathbb{E} \|\nabla_\ell\|^2 \\ &= \frac{1}{1-\rho\mathcal{T}} \sum_{\ell=0}^{t-1} (\rho\mathcal{T})^{\lceil \frac{t-\ell}{\mathcal{T}} \rceil} \mathbb{E} \|\nabla_\ell\|^2 \end{aligned}$$

Plugging this bound and Eq. (15) back to Eq. (14) gives

$$\begin{aligned} \mathbb{E}[f(w_{t+1}) - f(w_t)] &\leq \left(-\frac{\eta}{2} + 2\gamma\beta\eta^2 \right) \mathbb{E} \|\nabla_t\|^2 + \left(\frac{\beta\eta^2}{2} + 3\alpha \left(\frac{\beta^2\eta}{2} + \beta^3\eta^2 \right) \right) \tilde{\sigma}_S^2 \\ &\quad + (\eta + 2\beta\eta^2) \frac{\gamma}{(1-\rho\mathcal{T})\mathcal{T}} \sum_{k=0}^{t-1} (\rho\mathcal{T})^{\lceil \frac{t-k}{\mathcal{T}} \rceil} \mathbb{E} \|\nabla_k\|^2 . \end{aligned}$$

Summing over $t = 0, \dots, T-1$, we obtain

$$\begin{aligned} \mathbb{E}[f(w_T) - f(w_0)] &= \sum_{t=0}^{T-1} \mathbb{E}[f(w_{t+1}) - f(w_t)] \\ &\leq \left(-\frac{\eta}{2} + 2\gamma\beta\eta^2 \right) \sum_{t=0}^{T-1} \mathbb{E} \|\nabla_t\|^2 + \left(\frac{\beta\eta^2}{2} + 3\alpha \left(\frac{\beta^2\eta}{2} + \beta^3\eta^2 \right) \right) T\tilde{\sigma}_S^2 \\ &\quad + (\eta + 2\beta\eta^2) \frac{\gamma}{(1-\rho\mathcal{T})\mathcal{T}} \underbrace{\sum_{t=0}^{T-1} \sum_{k=0}^{t-1} (\rho\mathcal{T})^{\lceil \frac{t-k}{\mathcal{T}} \rceil} \mathbb{E} \|\nabla_k\|^2}_{=(C)} . \end{aligned} \quad (16)$$

Focusing on (C), we can change the outer summation bounds as

$$\sum_{t=0}^{T-1} \sum_{k=0}^{t-1} (\rho\mathcal{T})^{\lceil \frac{t-k}{\mathcal{T}} \rceil} \mathbb{E} \|\nabla_k\|^2 = \sum_{t=1}^{T-1} \sum_{k=0}^{t-1} (\rho\mathcal{T})^{\lceil \frac{t-k}{\mathcal{T}} \rceil} \mathbb{E} \|\nabla_k\|^2 \leq \sum_{t=1}^T \sum_{k=0}^{t-1} (\rho\mathcal{T})^{\lceil \frac{t-k}{\mathcal{T}} \rceil} \mathbb{E} \|\nabla_k\|^2 . \quad (17)$$

Now, we can bound the right-hand side using Lemma C.8 with $a = \rho\mathcal{T} < 1$ and $x_k = \mathbb{E} \|\nabla_k\|^2 \geq 0$ to get that

$$\sum_{t=1}^T \sum_{k=0}^{t-1} (\rho\mathcal{T})^{\lceil \frac{t-k}{\mathcal{T}} \rceil} \mathbb{E} \|\nabla_k\|^2 \leq \mathcal{T} \frac{\rho\mathcal{T}}{1-\rho\mathcal{T}} \sum_{t=0}^{T-1} \mathbb{E} \|\nabla_t\|^2 .$$

Plugging this bound back to Eq. (16) and using $\frac{1}{(1-\rho\mathcal{T})^2} \leq 4$ gives

$$\begin{aligned}
\mathbb{E}[f(w_T) - f(w_0)] &\leq \left(-\frac{\eta}{2} + 2\gamma\beta\eta^2\right) \sum_{t=0}^{T-1} \mathbb{E} \|\nabla_t\|^2 + \left(\frac{\beta\eta^2}{2} + 3\alpha \left(\frac{\beta^2\eta}{2} + \beta^3\eta^2\right)\right) T\tilde{\sigma}_S^2 \\
&\quad + (\eta + 2\beta\eta^2) \frac{\gamma\rho\mathcal{T}}{(1-\rho\mathcal{T})^2} \sum_{t=0}^{T-1} \mathbb{E} \|\nabla_t\|^2 \\
&\leq \left(-\frac{\eta}{2} + 2\gamma\beta\eta^2 + 4\gamma\rho\mathcal{T}(\eta + 2\beta\eta^2)\right) \sum_{t=0}^{T-1} \mathbb{E} \|\nabla_t\|^2 \\
&\quad + \left(\frac{\beta\eta^2}{2} + \frac{3\alpha\beta^2}{2}(\eta + 2\beta\eta^2)\right) T\tilde{\sigma}_S^2 \\
&\leq \left(-\frac{\eta}{2} + 2\gamma\beta\eta^2 + 8\gamma\rho\mathcal{T}\eta\right) \sum_{t=0}^{T-1} \mathbb{E} \|\nabla_t\|^2 + \left(\frac{\beta\eta^2}{2} + 3\alpha\beta^2\eta\right) T\tilde{\sigma}_S^2,
\end{aligned}$$

where in the last inequality we used the fact that $\eta \leq \frac{1}{30\gamma\beta\theta} \leq \frac{1}{30\beta}$ to bound $2\beta\eta^2 \leq \eta$.
Substituting α and ρ , we obtain:

$$\begin{aligned}
\mathbb{E}[f(w_T) - f(w_0)] &\leq \left(-\frac{\eta}{2} + 2\gamma\beta\eta^2 + 160\gamma\beta^2\omega^2\mathcal{T}^2\eta^3\right) \sum_{t=0}^{T-1} \mathbb{E} \|\nabla_t\|^2 \\
&\quad + \left(\frac{\beta\eta^2}{2} + 12\beta^2\omega^2\mathcal{T}\eta^3\right) T\tilde{\sigma}_S^2.
\end{aligned}$$

Since $\eta \leq \frac{1}{30\gamma\beta\theta}$, we can bound the coefficient of $\sum_{t=0}^{T-1} \mathbb{E} \|\nabla_t\|^2$ using Lemma C.9. We get:

$$\mathbb{E}[f(w_T) - f(w_0)] \leq -\frac{\eta}{4} \sum_{t=0}^{T-1} \mathbb{E} \|\nabla_t\|^2 + \left(\frac{\beta\eta^2}{2} + 12\beta^2\omega^2\mathcal{T}\eta^3\right) T\tilde{\sigma}_S^2. \quad (18)$$

Rearranging terms, multiplying by $4/\eta T$, and plugging $\tilde{\sigma}_S^2 = \tilde{\sigma}^2/S$ then gives

$$\mathbb{E} \left[\frac{1}{T} \sum_{t=0}^{T-1} \|\nabla_t\|^2 \right] \leq \frac{4M}{\eta T} + \frac{2\beta\tilde{\sigma}^2}{S}\eta + \frac{48\beta^2\omega^2\mathcal{T}\tilde{\sigma}^2}{S}\eta^2,$$

where we also used $\mathbb{E}[f(w_0) - f(w_T)] \leq f(w_0) - f^* \leq M$. Applying Lemma C.10 with our learning rate η , we finally obtain:

$$\begin{aligned}
\mathbb{E} \left[\frac{1}{T} \sum_{t=0}^{T-1} \|\nabla_t\|^2 \right] &\leq \frac{4M}{T} \left(30\gamma\beta\theta + \sqrt{\frac{\beta\tilde{\sigma}^2 T}{2MS}} + \left(\frac{12\beta^2\omega^2\mathcal{T}\tilde{\sigma}^2 T}{MS} \right)^{1/3} \right) + \frac{2\beta\tilde{\sigma}^2}{S} \cdot \sqrt{\frac{2MS}{\beta\tilde{\sigma}^2 T}} \\
&\quad + \frac{48\beta^2\omega^2\mathcal{T}\tilde{\sigma}^2}{S} \cdot \left(\frac{MS}{12\beta^2\omega^2\mathcal{T}\tilde{\sigma}^2 T} \right)^{2/3} \\
&= 4\sqrt{\frac{2M\beta\tilde{\sigma}^2}{TS}} + 8\frac{(12M^2\beta^2\omega^2\mathcal{T}\tilde{\sigma}^2)^{1/3}}{T^{2/3}S^{1/3}} + \frac{120\gamma\beta\theta}{T},
\end{aligned}$$

which concludes the proof. □

C.2 Technical Lemmata

In this section, we introduce some technical results used throughout our analysis. We start with the following lemma, yielding a bound on the second moment of the aggregated gradients that our PS uses to update its model.

Lemma C.1. *Consider the notations of Theorem 1. For every $t \in [T]$, it holds that*

$$\mathbb{E} \|\hat{g}_t\|^2 \leq \tilde{\sigma}_S^2 + 4\gamma \mathbb{E} \|\nabla_t\|^2 + 2\beta^2 \cdot \frac{1}{N} \sum_{i=1}^N \mathbb{E} \|\hat{w}_t^i - w_t\|^2. \quad (19)$$

Proof. Since \hat{g}_t is an aggregation of local gradient, we can write,

$$\begin{aligned} \mathbb{E} \|\hat{g}_t\|^2 &= \mathbb{E} \left\| \frac{1}{S} \sum_{i \in \mathcal{S}_t} \hat{g}_t^i \right\|^2 = \mathbb{E} \left\| \frac{1}{S} \sum_{i \in \mathcal{S}_t} (\hat{g}_t^i - \nabla f_i(\hat{w}_t^i) + \nabla f_i(\hat{w}_t^i)) \right\|^2 \\ &= \mathbb{E} \left\| \frac{1}{S} \sum_{i \in \mathcal{S}_t} (\hat{g}_t^i - \nabla f_i(\hat{w}_t^i)) \right\|^2 + \mathbb{E} \left\| \frac{1}{S} \sum_{i \in \mathcal{S}_t} \nabla f_i(\hat{w}_t^i) \right\|^2, \end{aligned}$$

where the last equality follows from Assumption 3.1 as $\mathbb{E}[(\hat{g}_t^i(\hat{w}_t^i) - \nabla f_i(\hat{w}_t^i))^\top \nabla f_i(\hat{w}_t^i)] = 0$. Note that the first term in the right-hand side is the variance of the average of S independent random variables with zero mean and variance bounded by σ^2 ; therefore, it is bounded by σ^2/S . Thus, we get that

$$\mathbb{E} \|\hat{g}_t\|^2 \leq \frac{\sigma^2}{S} + \mathbb{E} \left\| \frac{1}{S} \sum_{i \in \mathcal{S}_t} \nabla f_i(\hat{w}_t^i) \right\|^2. \quad (20)$$

Focusing on the second term in the right-hand side, we have that

$$\mathbb{E} \left\| \frac{1}{S} \sum_{i \in \mathcal{S}_t} \nabla f_i(\hat{w}_t^i) \right\|^2 \leq \underbrace{2\mathbb{E} \left\| \frac{1}{S} \sum_{i \in \mathcal{S}_t} (\nabla f_i(\hat{w}_t^i) - \nabla f_i(w_t)) \right\|^2}_{(A)} + \underbrace{2\mathbb{E} \left\| \frac{1}{S} \sum_{i \in \mathcal{S}_t} \nabla f_i(w_t) \right\|^2}_{=(B)}, \quad (21)$$

where we used the inequality $\|a + b\|^2 \leq 2\|a\|^2 + 2\|b\|^2$.

Bounding (A): Using Lemma C.5 and the β -smoothness of the objective, we get that

$$\begin{aligned}
2\mathbb{E} \left\| \frac{1}{S} \sum_{i \in \mathcal{S}_t} (\nabla f_i(\hat{w}_t^i) - \nabla f_i(w_t)) \right\|^2 &\leq \frac{2}{S} \mathbb{E} \left[\sum_{i \in \mathcal{S}_t} \|\nabla f_i(\hat{w}_t^i) - \nabla f_i(w_t)\|^2 \right] \\
&\leq \frac{2\beta^2}{S} \mathbb{E} \left[\sum_{i \in \mathcal{S}_t} \|\hat{w}_t^i - w_t\|^2 \right] \\
&= \frac{2\beta^2}{S} \mathbb{E} \left[\sum_{i=1}^N \|\hat{w}_t^i - w_t\|^2 \cdot \mathbb{1}_{\{i \in \mathcal{S}_t\}} \right] \\
&= \frac{2\beta^2}{N} \sum_{i=1}^N \mathbb{E} \|\hat{w}_t^i - w_t\|^2,
\end{aligned}$$

where the last equality follows from our assumption about the client participation process $\mathcal{P}(\cdot)$, which guarantees that $\mathbb{P}(i \in \mathcal{S}_t) = S/N$, independently of the optimization process.

Bounding (B): By the law of total expectation, (B) can be written as follows,

$$\begin{aligned}
2\mathbb{E} \left\| \frac{1}{S} \sum_{i \in \mathcal{S}_t} \nabla f_i(w_t) \right\|^2 &= 2\mathbb{E} \left\| \sum_{i=1}^N \left(\frac{1}{S} \nabla f_i(w_t) \cdot \mathbb{1}_{\{i \in \mathcal{S}_t\}} \right) \right\|^2 \\
&= 2\mathbb{E} \left[\mathbb{E} \left[\left\| \sum_{i=1}^N \left(\frac{1}{S} \nabla f_i(w_t) \cdot \mathbb{1}_{\{i \in \mathcal{S}_t\}} \right) \right\|^2 \middle| w_t \right] \right]. \tag{22}
\end{aligned}$$

Thus, we can use Lemma C.4 with $X_i = \frac{1}{S} \nabla f_i(w_t) \cdot \mathbb{1}_{\{i \in \mathcal{S}_t\}}$, $i \in [N]$ to bound the inner expectation. Using $\mathbb{P}(i \in \mathcal{S}_t) = S/N$, we have that

$$\mathbb{E}[X_i | w_t] = \frac{1}{S} \nabla f_i(w_t) \cdot \frac{S}{N} = \frac{1}{N} \nabla f_i(w_t),$$

and,

$$\begin{aligned}
\mathbb{E}[\|X_i - \mathbb{E}[X_i | w_t]\|^2 | w_t] &= \|\nabla f_i(w_t)\|^2 \cdot \mathbb{E} \left[\left(\frac{1}{S} \cdot \mathbb{1}_{\{i \in \mathcal{S}_t\}} - \frac{1}{N} \right)^2 \right] \\
&= \|\nabla f_i(w_t)\|^2 \cdot \text{Var} \left(\frac{1}{S} \cdot \mathbb{1}_{\{i \in \mathcal{S}_t\}} \right) \\
&= \frac{\|\nabla f_i(w_t)\|^2}{S^2} \cdot \frac{S}{N} \left(1 - \frac{S}{N} \right) = \frac{\|\nabla f_i(w_t)\|^2}{SN} \left(1 - \frac{S}{N} \right),
\end{aligned}$$

where we used the fact that for any event \mathcal{A} , the following holds: $\text{Var}(\mathbb{1}_{\mathcal{A}}) = \mathbb{P}(\mathcal{A}) \cdot (1 - \mathbb{P}(\mathcal{A}))$. Therefore, using Lemma C.4, we obtain that

$$\begin{aligned} \mathbb{E} \left[\left\| \sum_{i=1}^N \left(\frac{1}{S} \nabla f_i(w_t) \cdot \mathbb{1}_{\{i \in \mathcal{S}_t\}} \right) \right\|^2 \middle| w_t \right] &\leq 2 \left\| \frac{1}{N} \sum_{i=1}^N \nabla f_i(w_t) \right\|^2 \\ &\quad + \frac{2}{SN} \left(1 - \frac{S}{N} \right) \sum_{i=1}^N \|\nabla f_i(w_t)\|^2 \\ &\leq 2 \|\nabla_t\|^2 + \frac{2}{S} \left(1 - \frac{S}{N} \right) (G^2 + B^2 \|\nabla_t\|^2) \\ &= \left(1 - \frac{S}{N} \right) \frac{2G^2}{S} + 2 \underbrace{\left(1 + \left(1 - \frac{S}{N} \right) \frac{B^2}{S} \right)}_{:=\gamma} \|\nabla_t\|^2, \end{aligned}$$

where in the second inequality we used the bounded gradient dissimilarity assumption (Assumption 3.2). Plugging back to Eq. (22), we get the following bound on (B):

$$2\mathbb{E} \left\| \frac{1}{S} \sum_{i \in \mathcal{S}_t} \nabla f_i(w_t) \right\|^2 \leq \left(1 - \frac{S}{N} \right) \frac{4G^2}{S} + 4\gamma \mathbb{E} \|\nabla_t\|^2.$$

Plugging the bounds on (A) and (B) in Eq. (20) finally gives

$$\begin{aligned} \mathbb{E} \|\hat{g}_t\|^2 &\leq \underbrace{\frac{\sigma^2}{S} + \left(1 - \frac{S}{N} \right) \frac{4G^2}{S}}_{=\tilde{\sigma}^2/S} + 4\gamma \mathbb{E} \|\nabla_t\|^2 + \frac{2\beta^2}{N} \sum_{i=1}^N \mathbb{E} \|\hat{w}_t^i - w_t\|^2 \\ &= \tilde{\sigma}_S^2 + 4\gamma \mathbb{E} \|\nabla_t\|^2 + \frac{2\beta^2}{N} \sum_{i=1}^N \mathbb{E} \|\hat{w}_t^i - w_t\|^2, \end{aligned}$$

which concludes the proof. \square

The next result establishes a bound on the model estimation error of the clients.

Lemma C.2. *Consider the notations of Theorem 1. Let $\alpha := 4\omega^2\eta^2\mathcal{T}$, $\rho := 20\beta^2\omega^2\eta^2\mathcal{T}$, and $\nabla_{-\ell} := 0$, $\forall \ell \in \mathbb{N}$. Then, the following result holds:*

$$\frac{1}{N} \sum_{i=1}^N \mathbb{E} \|\hat{w}_t^i - w_t\|^2 \leq \alpha \left(1 + \sum_{k=1}^t k(\rho\mathcal{T})^k \right) \tilde{\sigma}_S^2 + \frac{2\gamma}{\beta^2\mathcal{T}} \sum_{k=1}^t (\rho\mathcal{T})^k \sum_{\ell=t-k\mathcal{T}}^{t-k} \mathbb{E} \|\nabla_\ell\|^2$$

Proof. We use strong induction. Particularly, to prove the result holds at round t , we rely on its correctness over the \mathcal{T} prior rounds, i.e., for every $s = t - \mathcal{T}, \dots, t - 1$. Thus, in our base case, we show that the result holds up to round \mathcal{T} .

We start with some general observations that hold for any t . Recall that $\hat{w}_t^i = y_t^i + \mathcal{C}(w_t - y_t^i)$. From Assumption 3.3, we have

$$\mathbb{E} \|\hat{w}_t^i - w_t\|^2 = \mathbb{E} \|\mathcal{C}_c(w_t - y_t^i) - (w_t - y_t^i)\|^2 \leq \omega^2 \mathbb{E} \|w_t - y_t^i\|^2. \quad (23)$$

Unrolling the update rule for w_t , we have for all $i \in [N]$ that

$$w_t = w_{t-\tau_t^i} - \eta \sum_{k=t-\tau_t^i}^{t-1} \hat{g}_k = y_t^i - \eta \sum_{k=t-\tau_t^i}^{t-1} \hat{g}_k.$$

Let $\hat{g}_{-k} := 0$ for all $k \in \mathbb{N}$. Additionally, let $\hat{\xi}_k = \hat{g}_k - \hat{\nabla}_k$ for all k , where $\hat{\nabla}_k = \mathbb{E}[\hat{g}_k]$, as defined in the proof of Theorem 1. Plugging back to Eq. (23), we get that

$$\mathbb{E} \|\hat{w}_t^i - w_t\|^2 \leq \omega^2 \eta^2 \mathbb{E} \left\| \sum_{k=t-\tau_t^i}^{t-1} \hat{g}_k \right\|^2 \leq 2\omega^2 \eta^2 \mathbb{E} \left\| \sum_{k=t-\tau_t^i}^{t-1} \hat{\nabla}_k \right\|^2 + 2\omega^2 \eta^2 \mathbb{E} \left\| \sum_{k=t-\tau_t^i}^{t-1} \hat{\xi}_k \right\|^2, \quad (24)$$

where the last inequality follows from $\|a + b\|^2 \leq 2\|a\|^2 + 2\|b\|^2$. Using Lemma C.5, we can bound the first term in the right-hand side, as

$$\mathbb{E} \left\| \sum_{k=t-\tau_t^i}^{t-1} \hat{\nabla}_k \right\|^2 \leq \tau_t^i \sum_{k=t-\tau_t^i}^{t-1} \mathbb{E} \|\hat{\nabla}_k\|^2 \leq \mathcal{T} \sum_{k=t-\mathcal{T}}^{t-1} \mathbb{E} \|\hat{\nabla}_k\|^2,$$

where the last inequality follows from $\tau_t^i \leq \mathcal{T}$. Since $\mathbb{E}[\hat{\xi}_k] = 0$, and $\mathbb{E}[\hat{\xi}_k^\top \hat{\xi}_\ell] = 0$ for all k, ℓ , we can apply Lemma C.3 to bound the second term in the right-hand side as follows:

$$\mathbb{E} \left\| \sum_{k=t-\tau_t^i}^{t-1} \hat{\xi}_k \right\|^2 = \sum_{k=t-\tau_t^i}^{t-1} \mathbb{E} \|\hat{\xi}_k\|^2 \leq \sum_{k=t-\mathcal{T}}^{t-1} \mathbb{E} \|\hat{\xi}_k\|^2 \leq 2 \sum_{k=t-\mathcal{T}}^{t-1} \mathbb{E} \|\hat{\nabla}_k\|^2 + 2 \sum_{k=t-\mathcal{T}}^{t-1} \mathbb{E} \|\hat{g}_k\|^2,$$

where we used $\tau_t^i \leq \mathcal{T}$, and $\|a - b\|^2 \leq 2\|a\|^2 + 2\|b\|^2$.

Plugging-in both bounds to Eq. (24), we obtain:

$$\begin{aligned} \mathbb{E} \|\hat{w}_t^i - w_t\|^2 &\leq (2\omega^2 \eta^2 \mathcal{T} + 4\omega^2 \eta^2) \sum_{k=t-\mathcal{T}}^{t-1} \mathbb{E} \|\hat{\nabla}_k\|^2 + 4\omega^2 \eta^2 \sum_{k=t-\mathcal{T}}^{t-1} \mathbb{E} \|\hat{g}_k\|^2 \\ &\leq 6\omega^2 \eta^2 \mathcal{T} \sum_{k=t-\mathcal{T}}^{t-1} \mathbb{E} \|\hat{\nabla}_k\|^2 + 4\omega^2 \eta^2 \sum_{k=t-\mathcal{T}}^{t-1} \mathbb{E} \|\hat{g}_k\|^2. \end{aligned} \quad (25)$$

Note that we can bound $\mathbb{E} \|\hat{\nabla}_k\|^2$ as:

$$\mathbb{E} \|\hat{\nabla}_k\|^2 \leq 2\mathbb{E} \|\hat{\nabla}_k - \nabla_k\|^2 + 2\mathbb{E} \|\nabla_k\|^2 \leq \frac{2\beta^2}{N} \sum_{i=1}^N \mathbb{E} \|\hat{w}_k^i - w_k\|^2 + 2\mathbb{E} \|\nabla_k\|^2,$$

where in the last inequality we used Eq. (13) to bound $\mathbb{E}\|\hat{\nabla}_k - \nabla_k\|^2$.

For the ease of notation, denote: $e_t^i := \mathbb{E}\|\hat{w}_t^i - w_t\|^2$, and $e_t := \frac{1}{N} \sum_{i=1}^N e_t^i$. Therefore, we obtain from Eq. (25) that

$$e_t^i \leq 12\beta^2\omega^2\eta^2\mathcal{T} \sum_{k=t-\mathcal{T}}^{t-1} e_k + 12\omega^2\eta^2\mathcal{T} \sum_{k=t-\mathcal{T}}^{t-1} \mathbb{E}\|\nabla_k\|^2 + 4\omega^2\eta^2 \sum_{k=t-\mathcal{T}}^{t-1} \mathbb{E}\|\hat{g}_k\|^2. \quad (26)$$

Base Case: For $t = 0$, each client obtains the exact model weights, i.e., $\hat{w}_0^i = w_0$, which trivially implies result. For every $t = 1, \dots, \mathcal{T}$ and $i \in [N]$, we have from Eq. (26) that

$$e_t^i \leq 12\beta^2\omega^2\eta^2\mathcal{T} \sum_{k=0}^{t-1} e_k + 12\omega^2\eta^2\mathcal{T} \sum_{k=0}^{t-1} \mathbb{E}\|\nabla_k\|^2 + 4\omega^2\eta^2 \sum_{k=0}^{t-1} \mathbb{E}\|\hat{g}_k\|^2. \quad (27)$$

Using Lemma C.1 to bound $\mathbb{E}\|\hat{g}_k\|^2$, we get:

$$\begin{aligned} e_t^i &\leq 12\beta^2\omega^2\eta^2\mathcal{T} \sum_{k=0}^{t-1} e_k + 12\omega^2\eta^2\mathcal{T} \sum_{k=0}^{t-1} \mathbb{E}\|\nabla_k\|^2 + 4\omega^2\eta^2 \sum_{k=0}^{t-1} (\tilde{\sigma}_S^2 + 4\gamma\mathbb{E}\|\nabla_k\|^2 + 2\beta^2 e_k) \\ &\leq 4\omega^2\eta^2\mathcal{T}\tilde{\sigma}_S^2 + (12\omega^2\eta^2\mathcal{T} + 16\gamma\omega^2\eta^2) \sum_{k=0}^{t-1} \mathbb{E}\|\nabla_k\|^2 + (12\beta^2\omega^2\eta^2\mathcal{T} + 8\beta^2\omega^2\eta^2) \sum_{k=0}^{t-1} e_k \\ &\leq 4\omega^2\eta^2\mathcal{T}\tilde{\sigma}_S^2 + 28\gamma\omega^2\eta^2\mathcal{T} \sum_{k=0}^{t-1} \mathbb{E}\|\nabla_k\|^2 + 20\beta^2\omega^2\eta^2\mathcal{T} \sum_{k=0}^{t-1} e_k. \end{aligned}$$

Note that this bound on e_t^i is independent of i , and thus, it holds for the average of e_t^i over $i \in [N]$, namely, e_t . Therefore, Eq. (26) implies a recursive bound on e_t ; for every $t = 1, \dots, \mathcal{T}$:

$$e_t \leq \alpha\tilde{\sigma}_S^2 + \nu \sum_{k=0}^{t-1} \mathbb{E}\|\nabla_k\|^2 + \rho \sum_{k=0}^{t-1} e_k, \quad (28)$$

where we denoted $\nu := 28\gamma\omega^2\eta^2\mathcal{T}$. Plugging-in this bound instead of e_k in the right-hand side, we obtain:

$$\begin{aligned} e_t &\leq \alpha\tilde{\sigma}_S^2 + \nu \sum_{k=0}^{t-1} \mathbb{E}\|\nabla_k\|^2 + \rho \sum_{k=0}^{t-1} \left(\alpha\tilde{\sigma}_S^2 + \nu \sum_{\ell=0}^{k-1} \mathbb{E}\|\nabla_\ell\|^2 + \rho \sum_{\ell=0}^{k-1} e_\ell \right) \\ &\leq \alpha(1 + \rho\mathcal{T})\tilde{\sigma}_S^2 + \nu \sum_{k=0}^{t-1} \mathbb{E}\|\nabla_k\|^2 + \nu\rho \sum_{k=0}^{t-1} \sum_{\ell=0}^{k-1} \mathbb{E}\|\nabla_\ell\|^2 + \rho^2 \sum_{k=0}^{t-1} \sum_{\ell=0}^{k-1} e_\ell, \end{aligned}$$

where we used $t \leq \mathcal{T}$. Note that we can bound the double sums in right-hand side using Lemma C.6 as

$$\sum_{k=0}^{t-1} \sum_{\ell=0}^{k-1} \mathbb{E}\|\nabla_\ell\|^2 \leq t \sum_{k=0}^{t-2} \mathbb{E}\|\nabla_k\|^2 \leq \mathcal{T} \sum_{k=0}^{t-2} \mathbb{E}\|\nabla_k\|^2,$$

and similarly,

$$\sum_{k=0}^{t-1} \sum_{\ell=0}^{k-1} e_{\ell} \leq \mathcal{T} \sum_{k=0}^{t-2} e_k .$$

Plugging-back, we get:

$$e_t \leq \alpha (1 + \rho\mathcal{T}) \tilde{\sigma}_S^2 + \nu \sum_{k=0}^{t-1} \mathbb{E} \|\nabla_k\|^2 + \nu \rho \mathcal{T} \sum_{k=0}^{t-2} \mathbb{E} \|\nabla_{\ell}\|^2 + \rho^2 \mathcal{T} \sum_{k=0}^{t-2} e_k .$$

We can once again apply Eq. (28) to bound e_k , and obtain:

$$\begin{aligned} e_t &\leq \alpha (1 + \rho\mathcal{T}) \tilde{\sigma}_S^2 + \nu \sum_{k=0}^{t-1} \mathbb{E} \|\nabla_k\|^2 + \nu \rho \mathcal{T} \sum_{k=0}^{t-2} \mathbb{E} \|\nabla_{\ell}\|^2 \\ &\quad + \rho^2 \mathcal{T} \sum_{k=0}^{t-2} \left(\alpha \tilde{\sigma}_S^2 + \nu \sum_{\ell=0}^{k-1} \mathbb{E} \|\nabla_{\ell}\|^2 + \rho \sum_{\ell=0}^{k-1} e_{\ell} \right) \\ &\leq \alpha (1 + \rho\mathcal{T} + \rho^2 \mathcal{T}^2) \tilde{\sigma}_S^2 + \nu \sum_{k=0}^{t-1} \mathbb{E} \|\nabla_k\|^2 + \nu \rho \mathcal{T} \sum_{k=0}^{t-2} \mathbb{E} \|\nabla_{\ell}\|^2 + \nu \rho^2 \mathcal{T} \sum_{k=0}^{t-2} \sum_{\ell=0}^{k-1} \mathbb{E} \|\nabla_{\ell}\|^2 \\ &\quad + \rho^3 \mathcal{T} \sum_{k=0}^{t-2} \sum_{\ell=0}^{k-1} e_{\ell} \\ &\leq \alpha (1 + \rho\mathcal{T} + \rho^2 \mathcal{T}^2) \tilde{\sigma}_S^2 + \nu \sum_{k=0}^{t-1} \mathbb{E} \|\nabla_k\|^2 + \nu \rho \mathcal{T} \sum_{k=0}^{t-2} \mathbb{E} \|\nabla_{\ell}\|^2 + \nu \rho^2 \mathcal{T}^2 \sum_{k=0}^{t-3} \mathbb{E} \|\nabla_{\ell}\|^2 + \rho^3 \mathcal{T}^2 \sum_{k=0}^{t-3} e_k , \end{aligned}$$

where in the last inequality we used Lemma C.6. Repeating this process of alternately applying Eq. (28) to bound e_k and Lemma C.6, finally gives:

$$e_t \leq \alpha \left(1 + \sum_{k=1}^t (\rho\mathcal{T})^k \right) \tilde{\sigma}_S^2 + \frac{\nu}{\rho\mathcal{T}} \sum_{k=1}^t (\rho\mathcal{T})^k \sum_{\ell=0}^{t-k} \mathbb{E} \|\nabla_{\ell}\|^2 .$$

Plugging ν and ρ , we can bound the coefficient $\nu/\rho\mathcal{T}$ as:

$$\frac{\nu}{\rho\mathcal{T}} = \frac{28\gamma\omega^2\eta^2\mathcal{T}}{20\beta^2\omega^2\eta^2\mathcal{T}^2} \leq \frac{2\gamma}{\beta^2\mathcal{T}} .$$

Using $(\rho\mathcal{T})^k \leq k(\rho\mathcal{T})^k$, which holds for any $k \geq 1$, we then obtain:

$$e_t \leq \alpha \left(1 + \sum_{k=1}^t k(\rho\mathcal{T})^k \right) \tilde{\sigma}_S^2 + \frac{2\gamma}{\beta^2\mathcal{T}} \sum_{k=1}^t (\rho\mathcal{T})^k \sum_{\ell=0}^{t-k} \mathbb{E} \|\nabla_{\ell}\|^2 .$$

Note that for all $t \leq \mathcal{T}$ and $k \geq 1$, we have $t - k\mathcal{T} \leq 0$. Therefore, since for $\nabla_{-\ell} = 0$ for all $\ell \in \mathbb{N}$, we can equivalently write:

$$e_t \leq \alpha \left(1 + \sum_{k=1}^t k(\rho\mathcal{T})^k \right) \tilde{\sigma}_S^2 + \frac{2\gamma}{\beta^2\mathcal{T}} \sum_{k=1}^t (\rho\mathcal{T})^k \sum_{\ell=t-k\mathcal{T}}^{t-k} \mathbb{E} \|\nabla_{\ell}\|^2 ,$$

which establishes the result for the base case.

Induction step: The induction hypothesis is that the following holds:

$$e_s \leq \alpha \left(1 + \sum_{k=1}^s k(\rho\mathcal{T})^k \right) \tilde{\sigma}_S^2 + \frac{2\gamma}{\beta^2\mathcal{T}} \sum_{k=1}^s (\rho\mathcal{T})^k \sum_{\ell=s-k\mathcal{T}}^{s-k} \mathbb{E}\|\nabla_\ell\|^2, \quad \forall s = t - \mathcal{T}, \dots, t - 1. \quad (29)$$

We focus on Eq. (26). Using Lemma C.1 to bound $\mathbb{E}\|\hat{g}_k\|^2$ and following similar steps to those used to derive Eq. (28), we get

$$\begin{aligned} e_t^i &\leq 12\beta^2\omega^2\eta^2\mathcal{T} \sum_{k=t-\mathcal{T}}^{t-1} e_k + 12\omega^2\eta^2\mathcal{T} \sum_{k=t-\mathcal{T}}^{t-1} \mathbb{E}\|\nabla_k\|^2 + 4\omega^2\eta^2 \sum_{k=t-\mathcal{T}}^{t-1} (\tilde{\sigma}_S^2 + 4\gamma\mathbb{E}\|\nabla_k\|^2 + 2\beta^2e_k) \\ &\leq \alpha\tilde{\sigma}_S^2 + \nu \sum_{k=t-\mathcal{T}}^{t-1} \mathbb{E}\|\nabla_k\|^2 + \rho \underbrace{\sum_{k=t-\mathcal{T}}^{t-1} e_k}_{=(\dagger)}. \end{aligned} \quad (30)$$

From the induction hypothesis (29), we can bound e_k for every $k \in [t - \mathcal{T}, t - 1]$ as follows:

$$e_k \leq \alpha \left(1 + \sum_{\ell=1}^k \ell(\rho\mathcal{T})^\ell \right) \tilde{\sigma}_S^2 + \frac{2\gamma}{\beta^2\mathcal{T}} \sum_{\ell=1}^k (\rho\mathcal{T})^\ell \sum_{m=k-\ell\mathcal{T}}^{k-\ell} \mathbb{E}\|\nabla_m\|^2.$$

Denote this bound by $B(k) := \alpha \left(1 + \sum_{\ell=1}^k \ell(\rho\mathcal{T})^\ell \right) \tilde{\sigma}_S^2 + \frac{2\gamma}{\beta^2\mathcal{T}} \sum_{\ell=1}^k (\rho\mathcal{T})^\ell \sum_{m=k-\ell\mathcal{T}}^{k-\ell} \mathbb{E}\|\nabla_m\|^2$; that is, $e_k \leq B(k)$. We can therefore bound (\dagger) as

$$\sum_{k=t-\mathcal{T}}^{t-1} e_k \leq \sum_{k=t-\mathcal{T}}^{t-1} B(k) \leq \mathcal{T}B(t-1),$$

where the last inequality holds because $B(k)$ is monotonically increasing. Plugging back to Eq. (30) and substituting $B(t-1)$ gives

$$\begin{aligned} e_t^i &\leq \alpha\tilde{\sigma}_S^2 + \nu \sum_{k=t-\mathcal{T}}^{t-1} \mathbb{E}\|\nabla_k\|^2 + \rho \cdot \mathcal{T}B(t-1) \\ &= \alpha\tilde{\sigma}_S^2 + \nu \sum_{k=t-\mathcal{T}}^{t-1} \mathbb{E}\|\nabla_k\|^2 + \rho\mathcal{T} \left(\alpha \left(1 + \sum_{k=1}^{t-1} k(\rho\mathcal{T})^k \right) \tilde{\sigma}_S^2 + \frac{2\gamma}{\beta^2\mathcal{T}} \sum_{k=1}^{t-1} (\rho\mathcal{T})^k \sum_{\ell=t-1-k\mathcal{T}}^{t-1-k} \mathbb{E}\|\nabla_\ell\|^2 \right) \\ &= \underbrace{\alpha \left(1 + \rho\mathcal{T} + \sum_{k=1}^{t-1} k(\rho\mathcal{T})^{k+1} \right) \tilde{\sigma}_S^2}_{=(A)} + \nu \underbrace{\sum_{k=t-\mathcal{T}}^{t-1} \mathbb{E}\|\nabla_k\|^2 + \frac{2\gamma}{\beta^2\mathcal{T}} \sum_{k=1}^{t-1} (\rho\mathcal{T})^{k+1} \sum_{\ell=t-1-k\mathcal{T}}^{t-1-k} \mathbb{E}\|\nabla_\ell\|^2}_{=(B)}. \end{aligned} \quad (31)$$

Bounding (A): Using simple algebra, we have that

$$\rho\mathcal{T} + \sum_{k=1}^{t-1} k(\rho\mathcal{T})^{k+1} = \rho\mathcal{T} + \sum_{k=2}^t (k-1)(\rho\mathcal{T})^k \leq \rho\mathcal{T} + \sum_{k=2}^t k(\rho\mathcal{T})^k = \sum_{k=1}^t k(\rho\mathcal{T})^k. \quad (32)$$

This implies that (A) is bounded by $\alpha(1 + \sum_{k=1}^t k(\rho\mathcal{T})^k)$.

Bounding (B): Focusing on the first term in (B), we can bound:

$$\nu \sum_{k=t-\mathcal{T}}^{t-1} \mathbb{E}\|\nabla_k\|^2 = \frac{\nu}{\rho\mathcal{T}} \cdot \rho\mathcal{T} \sum_{k=t-\mathcal{T}}^{t-1} \mathbb{E}\|\nabla_k\|^2 \leq \frac{2\gamma}{\beta^2\mathcal{T}} \cdot \rho\mathcal{T} \sum_{k=t-\mathcal{T}}^{t-1} \mathbb{E}\|\nabla_k\|^2. \quad (33)$$

Focusing on the second sum in (B), we can bound

$$\begin{aligned} \frac{2\gamma}{\beta^2\mathcal{T}} \sum_{k=1}^{t-1} (\rho\mathcal{T})^{k+1} \sum_{\ell=t-1-k\mathcal{T}}^{t-1-k} \mathbb{E}\|\nabla_\ell\|^2 &= \frac{2\gamma}{\beta^2\mathcal{T}} \sum_{k=2}^t (\rho\mathcal{T})^k \sum_{\ell=t-1-(k-1)\mathcal{T}}^{t-1-(k-1)} \mathbb{E}\|\nabla_\ell\|^2 \\ &= \frac{2\gamma}{\beta^2\mathcal{T}} \sum_{k=2}^t (\rho\mathcal{T})^k \sum_{\ell=t-k\mathcal{T}+\mathcal{T}-1}^{t-k} \mathbb{E}\|\nabla_\ell\|^2 \\ &\leq \frac{2\gamma}{\beta^2\mathcal{T}} \sum_{k=2}^t (\rho\mathcal{T})^k \sum_{\ell=t-k\mathcal{T}}^{t-k} \mathbb{E}\|\nabla_\ell\|^2, \end{aligned} \quad (34)$$

where the last inequality holds since $\mathcal{T} - 1 \geq 0$ and $\mathbb{E}\|\nabla_\ell\|^2 \geq 0$ for all ℓ . Combining the bounds in Eq. (33) and (34), we can then bound (B) as

$$\begin{aligned} \nu \sum_{k=t-\mathcal{T}}^{t-1} \mathbb{E}\|\nabla_k\|^2 + \frac{2\gamma}{\beta^2\mathcal{T}} \sum_{k=1}^{t-1} (\rho\mathcal{T})^{k+1} \sum_{\ell=t-1-k\mathcal{T}}^{t-1-k} \mathbb{E}\|\nabla_\ell\|^2 &\leq \frac{2\gamma}{\beta^2\mathcal{T}} \cdot \rho\mathcal{T} \sum_{k=t-\mathcal{T}}^{t-1} \mathbb{E}\|\nabla_k\|^2 \\ &\quad + \frac{2\gamma}{\beta^2\mathcal{T}} \sum_{k=2}^t (\rho\mathcal{T})^k \sum_{\ell=t-k\mathcal{T}}^{t-k} \mathbb{E}\|\nabla_\ell\|^2 \\ &= \frac{2\gamma}{\beta^2\mathcal{T}} \sum_{k=1}^t (\rho\mathcal{T})^k \sum_{\ell=t-k\mathcal{T}}^{t-k} \mathbb{E}\|\nabla_\ell\|^2. \end{aligned} \quad (35)$$

Plugging back to Eq. (31) the bounds on (A) and (B) (from Eq. (32) and (35), respectively), we get:

$$e_t^i \leq \alpha \left(1 + \sum_{k=1}^t k(\rho\mathcal{T})^k \right) \tilde{\sigma}_S^2 + \frac{2\gamma}{\beta^2\mathcal{T}} \sum_{k=1}^t (\rho\mathcal{T})^k \sum_{\ell=t-k\mathcal{T}}^{t-k} \mathbb{E}\|\nabla_\ell\|^2.$$

Since this bound is independent of i , it also holds for the average $e_t = \frac{1}{N} \sum_{i=1}^N e_t^i$, establishing the result. \square

Lemma C.3. Let $X_1, \dots, X_N \in \mathbb{R}^d$ be N orthogonal, zero mean random variables, i.e., $\mathbb{E}[X_i] = 0$ for all $i \in [N]$, and $\mathbb{E}[X_i^\top X_j] = 0$ for all $i \neq j$. Then, the following holds:

$$\mathbb{E} \left\| \sum_{i=1}^N X_i \right\|^2 = \sum_{i=1}^N \mathbb{E} \|X_i\|^2.$$

Proof.

$$\mathbb{E} \left\| \sum_{i=1}^N X_i \right\|^2 = \mathbb{E} \left[\sum_{i=1}^N \sum_{j=1}^N X_i^\top X_j \right] = \sum_{i=1}^N \mathbb{E} \|X_i\|^2,$$

where the last equality follows from the following property: $\mathbb{E}[X_i^\top X_j] = 0$, $\forall i \neq j$, and the linearity of expectation. \square

The following lemma establishes a bound on the second moment of the sum of random variables in terms of their means and variances.

Lemma C.4 (Lemma 4, [Karimireddy et al., 2020](#)). Let $X_1, \dots, X_N \in \mathbb{R}^d$ be N independent random variables. Suppose that $\mathbb{E}[X_i] = \mu_i$ and $\mathbb{E} \|X_i - \mu_i\|^2 \leq \sigma_i^2$. Then, the following holds

$$\mathbb{E} \left\| \sum_{i=1}^N X_i \right\|^2 \leq 2 \left\| \sum_{i=1}^N \mu_i \right\|^2 + 2 \sum_{i=1}^N \sigma_i^2.$$

Next, we state a simple result about the squared norm of the sum of vectors.

Lemma C.5. For any $u_1, \dots, u_N \in \mathbb{R}^d$, it holds that $\left\| \sum_{i=1}^N u_i \right\|^2 \leq N \sum_{i=1}^N \|u_i\|^2$.

Proof. By the convexity of $\|\cdot\|^2$ and Jensen's inequality, we have

$$\left\| \frac{1}{N} \sum_{i=1}^N u_i \right\|^2 \leq \frac{1}{N} \sum_{i=1}^N \|u_i\|^2,$$

which implies the result. \square

The next result is a simple bound on a double sum of non-negative numbers.

Lemma C.6. Let $t, \tau \in \mathbb{N}$ such that $t \geq \tau + 1$. For any sequence of non-negative numbers $x_0, x_1, \dots, x_{t-\tau-1}$, the following holds

$$\sum_{k=0}^{t-\tau} \sum_{\ell=0}^{k-1} x_\ell \leq t \cdot \sum_{k=0}^{t-\tau-1} x_k.$$

Proof. Immediately,

$$\sum_{k=0}^{t-\tau} \sum_{\ell=0}^{k-1} x_\ell = \sum_{k=0}^{t-\tau-1} (t-\tau-k)x_k \leq t \cdot \sum_{k=0}^{t-\tau-1} x_k .$$

□

The following lemma gives a bound on the derivative of a power series.

Lemma C.7. *Let $a < 1$. Then,*

$$\sum_{k=1}^{\infty} k a^k = \frac{a}{(1-a)^2} .$$

Proof. Let $f_k(a) = a^k$.

$$\sum_{k=1}^{\infty} k a^k = a \sum_{k=1}^{\infty} k a^{k-1} = a \sum_{k=1}^{\infty} f'_k(a) .$$

Using term-by-term differentiation [Stewart \(2015\)](#), we have that

$$\sum_{k=1}^{\infty} f'_k(a) = \left(\sum_{k=1}^{\infty} f_k(a) \right)' = \left(\sum_{k=1}^{\infty} a^k \right)' = \left(\frac{a}{1-a} \right)' = \frac{1}{(1-a)^2} .$$

Multiplying by a gives the result. □

Next, we state a non-trivial inequality to bound the double sum that appears on the right-hand side of Eq. (17).

Lemma C.8. *Let $a \in (0, 1)$ and $T, \mathcal{T} \in \mathbb{N}$. Moreover, let x_0, \dots, x_{T-1} be a sequence of non-negative numbers. Then,*

$$\sum_{t=1}^T \sum_{k=0}^{t-1} a^{\lceil \frac{t-k}{\mathcal{T}} \rceil} x_k \leq \mathcal{T} \frac{a}{1-a} \sum_{k=0}^{T-1} x_k .$$

Proof. We start with changing the order of summation in the left-hand side. Note that for any fixed k , the element x_k appears in the inner sum if $k \leq t-1$, or equivalently, $t \geq k+1$. Therefore,

$$\sum_{t=1}^T \sum_{k=0}^{t-1} a^{\lceil \frac{t-k}{\mathcal{T}} \rceil} x_k = \sum_{k=0}^{T-1} \left(\sum_{t=k+1}^T a^{\lceil \frac{t-k}{\mathcal{T}} \rceil} \right) x_k = \sum_{k=0}^{T-1} \left(\sum_{t=1}^{T-k} a^{\lceil \frac{t}{\mathcal{T}} \rceil} \right) x_k . \quad (36)$$

Focusing on the inner sum in the right-hand side, $\sum_{t=1}^{T-k} a^{\lceil t/\mathcal{T} \rceil}$, we can divide the interval of integers from 1 to $T-k$ into non-overlapping intervals of length \mathcal{T} (and possibly a small residual) and get that

$$\sum_{t=1}^{T-k} a^{\lceil \frac{t}{\mathcal{T}} \rceil} \leq \sum_{m=1}^{\lceil \frac{T-k}{\mathcal{T}} \rceil} \sum_{\ell=1}^{\mathcal{T}} a^{\lceil \frac{(m-1)\mathcal{T} + \ell}{\mathcal{T}} \rceil} \stackrel{(\dagger)}{=} \sum_{m=1}^{\lceil \frac{T-k}{\mathcal{T}} \rceil} \sum_{\ell=1}^{\mathcal{T}} a^m = \mathcal{T} \sum_{m=1}^{\lceil \frac{T-k}{\mathcal{T}} \rceil} a^m \leq \mathcal{T} \frac{a}{1-a} .$$

where (†) holds because for every $\ell = 1, \dots, \mathcal{T}$ we have $\lceil \frac{(m-1)\mathcal{T} + \ell}{\mathcal{T}} \rceil = m$, and the last inequality follows from $\sum_{m=1}^{\lceil \frac{\mathcal{T}-k}{\mathcal{T}} \rceil} a^m \leq \sum_{m=1}^{\infty} a^m = \frac{a}{1-a}$ as $a < 1$. Plugging back to Eq. (36) concludes the proof. \square

The next lemma establishes that for small enough η , we have $-\eta/2 + \mathcal{O}(\eta^2) \leq -\eta/4$.

Lemma C.9. *Let $\gamma, \theta \geq 1$. For every $\eta \leq \frac{1}{30\gamma\beta\theta}$, it holds that*

$$-\frac{\eta}{2} + 2\gamma\beta\eta^2 + 160\gamma\beta^2\theta^2\eta^3 \leq -\frac{\eta}{4}.$$

Proof. We equivalently prove that

$$2\gamma\beta\eta^2 + 160\gamma\beta^2\theta^2\eta^3 \leq \frac{\eta}{4}.$$

Since both $\gamma \geq 1$ and $\theta \geq 1$, we have

$$\begin{aligned} 2\gamma\beta\eta^2 + 160\gamma\beta^2\theta^2\eta^3 &\leq 2\gamma\beta\theta\eta^2 + 160\gamma^2\beta^2\theta^2\eta^3 \\ &= \frac{\eta}{4} (8\gamma\beta\theta\eta + 640\gamma^2\beta^2\theta^2\eta^2) \\ &\leq \frac{\eta}{4} \left(\frac{8\gamma\beta\theta}{30\gamma\beta\theta} + \frac{640\gamma^2\beta^2\theta^2}{900\gamma^2\beta^2\theta^2} \right) \\ &= \frac{\eta}{4} \cdot \frac{44}{45} \\ &\leq \frac{\eta}{4}, \end{aligned}$$

where the second inequality follows from the upper bound on η . \square

We also make use of the following result, which we prove using simple algebra.

Lemma C.10. *Suppose $\eta = \min\{\eta_1, \eta_2, \eta_3\}$ for some $\eta_1, \eta_2, \eta_3 > 0$, and let $A, B, C > 0$. Then, the following holds:*

$$\frac{A}{\eta} + B\eta + C\eta^2 \leq A \left(\frac{1}{\eta_1} + \frac{1}{\eta_2} + \frac{1}{\eta_3} \right) + B\eta_2 + C\eta_3^2.$$

Proof. Since η is the minimum of three terms, $1/\eta$ is the maximum of their inverses. Thus, we can bound $1/\eta$ by the sum of the inverses as follows:

$$\frac{A}{\eta} = A \max \left\{ \frac{1}{\eta_1}, \frac{1}{\eta_2}, \frac{1}{\eta_3} \right\} \leq A \left(\frac{1}{\eta_1} + \frac{1}{\eta_2} + \frac{1}{\eta_3} \right).$$

The terms $B\eta$ and $C\eta^2$ are monotonically increasing with η . We can therefore bound η by η_2 and η^2 by η_3^2 . \square

D Entropy-Constrained Uniform Quantization

In this section, we describe a new compression technique entitled Entropy-Constrained Uniform Quantization (ECUQ), which we developed for anchor compression, although it can be of independent interest. ECUQ is described in Algorithm 4.

Algorithm 4 Entropy-Constrained Uniform Quantization (ECUQ)

Input: Vector $x \in \mathbb{R}^d$, bandwidth budget b (bits/coordinate), tolerance ϵ .
 $x_{\max} \leftarrow \max_i x(i)$, $x_{\min} \leftarrow \min_i x(i)$ ▷ Get max/min values of input vector
 $K \leftarrow 2^b$, $\Delta \leftarrow (x_{\max} - x_{\min})/K$ ▷ Initialize # of quantization values and bin length
 $\mathcal{Q} \leftarrow \{x_{\min} + (k + \frac{1}{2}) \cdot \Delta : k = 0, \dots, K - 1\}$ ▷ Set uniformly spaced quantization values
 $\hat{x}_{\mathcal{Q}} \leftarrow \text{Quantize}(x, \mathcal{Q})$ ▷ $\hat{x}_{\mathcal{Q}}(i) = \arg \min_{q \in \mathcal{Q}} \|x(i) - q\|$
 $p \leftarrow \text{Empirical_Density}(\hat{x}_{\mathcal{Q}})$ ▷ $p(q) = \frac{1}{N} \sum_{i \in [N]} \mathbb{1}\{\hat{x}_{\mathcal{Q}}(i) = q\}$, $\forall q \in \mathcal{Q}$
 $\mathcal{H}(p) \leftarrow \text{Entropy}(p_{\mathcal{Q}})$ ▷ $\mathcal{H}(p) = - \sum_{q \in \mathcal{Q}} p_{\mathcal{Q}}(q) \log p_{\mathcal{Q}}(q)$
if $\mathcal{H}(p) < b - \epsilon$ **then**
 $\hat{x}_{\mathcal{Q}} \leftarrow \text{BINARY_SEARCH_NUM_QUANTIZATION_LEVELS}(x, b)$
end if
 $\hat{x}_e \leftarrow \text{Huffman_Coding}(\hat{x}_{\mathcal{Q}})$ ▷ Entropy encoding of the quantized vector
Return: \hat{x}_e

Procedure BINARY_SEARCH_NUM_QUANTIZATION_LEVELS(x, b)

Initialize: $\text{low} \leftarrow 2^b$, $\text{high} \leftarrow \infty$, $p \leftarrow -1$
while $\text{low} \leq \text{high}$ **do**
 if $\text{high} == \infty$ **then**
 $p \leftarrow p + 1$
 $\text{mid} \leftarrow 2^b + 2^p$ ▷ Increase # of levels exponentially
 else
 $\text{mid} \leftarrow (\text{low} + \text{high})/2$
 end if
 $K \leftarrow \text{mid}$, $\Delta \leftarrow (x_{\max} - x_{\min})/\text{mid}$
 $\mathcal{Q} \leftarrow \{x_{\min} + (k + \frac{1}{2}) \cdot \Delta : k = 0, \dots, K - 1\}$
 $\hat{x}_{\mathcal{Q}} \leftarrow \text{Quantize}(x, \mathcal{Q})$
 $p \leftarrow \text{Empirical_Density}(\hat{x}_{\mathcal{Q}})$
 $\mathcal{H}(p) \leftarrow \text{Entropy}(p_{\mathcal{Q}})$
 if $\mathcal{H}(p) > b$ **then**
 $\text{high} \leftarrow \text{mid} - 1$
 else if $\mathcal{H}(p) < b - \epsilon$ **then**
 $\text{low} \leftarrow \text{mid} + 1$
 else
 return $\hat{x}_{\mathcal{Q}}$
 end if

Let $x = (x(1), \dots, x(d)) \in \mathbb{R}^d$ be some input vector we wish to compress using ECUQ. Denote: $x_{\min} := \min_i x(i)$, $x_{\max} := \max_i x(i)$. Given some bandwidth budget of b bits/coordinate, ECUQ initially divided the interval $[x_{\min}, x_{\max}]$ into $K = 2^b$ non-overlapping bins of equal

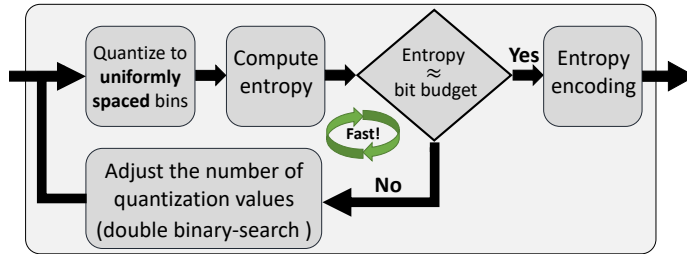


Figure 5: ECUQ encoder’s illustration.

size $\Delta = (x_{\max} - x_{\min})/K$. Then, it sets the quantization values, which we denote by \mathcal{Q} , to be the centers of these bins. Afterwards, the vector x is quantized into elements of \mathcal{Q} , that is, each element $x(i)$ is assigned to its closest quantization value $q \in \mathcal{Q}$ to generate the quantized vector $\hat{x}_{\mathcal{Q}}$, whose elements are all in \mathcal{Q} . We then compute the empirical distribution of the quantized vector by counting for every $q \in \mathcal{Q}$ the number of times it appears in $\hat{x}_{\mathcal{Q}}$, and the entropy of the resulting distribution. Note that the entropy is upper bounded by $\log K = b$. Finally, for some small tolerance parameter ϵ (we use $\epsilon = 0.1$), we check whether the entropy is within ϵ distance from the budget b : if it is not the case, then we perform a binary search, repeating the above procedure with increased number of quantization values K , to find the maximal number of uniformly spaced quantization values such that the entropy of the empirical distribution of the resulting quantized vector is within ϵ distance from b . Only after this entropy condition is satisfied, we encode $\hat{x}_{\mathcal{Q}}$ using some entropy encoding (we use Huffman coding).

Figure 5 illustrates the ECUQ’s encoder, as described in the text above. The corresponding decoder is fairly simple as it only performs entropy decoding in linear time (Huffman decoding).

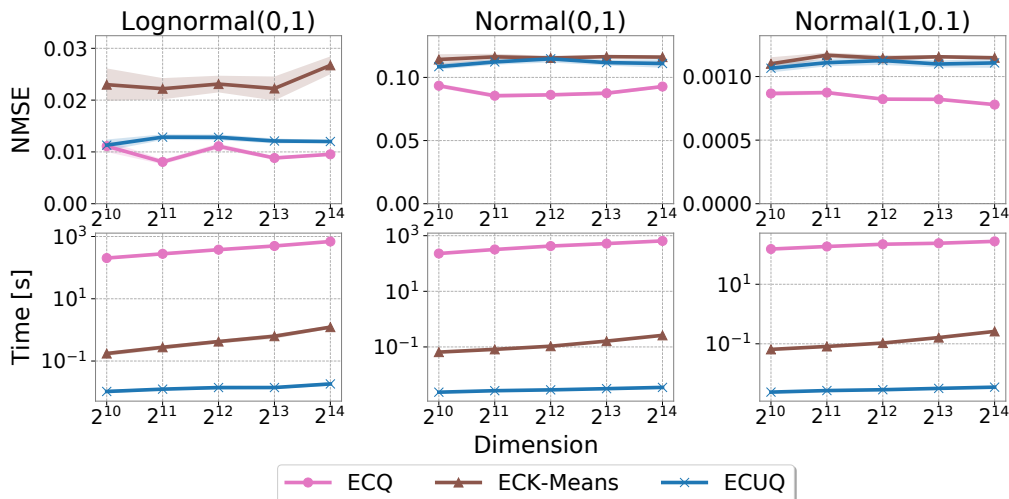


Figure 6: ECQ vs. ECK-Means vs. ECUQ: Normalized mean-squared-error (**top**) and encoding time (**bottom**) as a function of the input dimension for different input distributions and fixed bandwidth budget of 2 bits/coordinate.

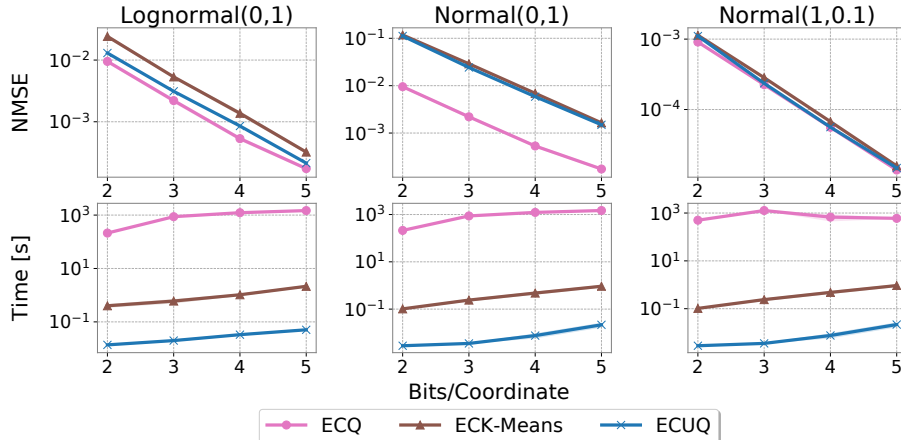


Figure 7: ECQ vs. ECK-Means vs. ECUQ: Normalized mean-squared-error (**top**) and encoding time (**bottom**) as a function of the bandwidth budget for different input distributions and fixed input dimension of $d = 2^{12}$.

During the process of devising ECUQ, we also considered an additional method to approximate ECQ. It is similar to ECUQ, but instead of using uniformly spaced quantization values, it uses K-Means clustering to find the quantization values that minimize the overall squared error. We used a binary search here as well to find the largest number of levels K such that, after entropy encoding, the bandwidth constraint is satisfied. We termed this method *Entropy-Constrained K-Means (ECK-Means)*.

We compare the performance of ECUQ with ECQ and ECK-Means in terms of their NMSE, and we also measure their encoding time. As we mentioned in the Section 4, ECQ is sensitive to hyperparameters; thus, we implemented it using a grid search over its hyperparameters to guarantee near-optimal performance.³ We evaluate the three methods on vectors drawn from three different synthetic distributions: **(1)** *LogNormal(0, 1)*; **(2)** *Normal(0, 1)*; and **(3)** *Normal(1, 0.1)*. In Figure 6 we show the NMSE and encoding time for different sizes of input vectors when the budget constraint is $b = 2$ bits/coordinate. As a complementary result, in Figure 7 we fix the dimension of the input vectors to $d = 2^{12} = 4096$ and vary the bandwidth budget constraint from 2 to 5 bits/coordinate.

The results imply that ECUQ exhibits a good speed-accuracy trade-off: it consistently outperforms ECK-Means while being an order of magnitude faster, and it is competitive with ECQ but about three orders of magnitude faster. Note additionally that it takes ≈ 20 minutes for ECQ to encode even a small vectors of size 2^{12} with budget constraint of 4 bits/coordinate (Fig. 7); this means that ECQ without some acceleration is not suitable for compressing neural networks with millions and even billions of parameters.

³While such implementation may increase the encoding time, we are not aware of any other approach to guarantee an optimal performance. ECQ aims at solving a hard non-convex problem, and different hyperparameters may result in different local minima.

E Experimental Details

We implemented DoCoFL in PyTorch [Paszke et al. \(2019\)](#). In all experiments, the PS uses Momentum SGD as optimizer with a momentum of 0.9 and L_2 regularization (i.e., weight decay) with parameter 10^{-5} . The clients, on the other hand, use vanilla SGD for all tasks but Amazon Reviews, for which Adam provided better results. In Table 4 we report the hyperparameters used in our experiments.

To ease the computational burden and long training times, in the Shakespeare task we reduced the amount of train and validation data for each speaker (i.e., client) by a factor of 10 by using only the first 10% of train and validation data, but no less than 2 samples per speaker.

Table 4: Hyperparameters for our experiments.

Task	Batch size	Client optimizer	Client lr	Server lr
EMNIST	64	SGD	0.05	1
CIFAR-100	128	SGD	0.05	1
Amazon Review	64	Adam	0.005	0.1
Shakespeare	4	SGD	0.5	1

F Additional Results

In this section, we provide the learning curves for the experiments we conducted. In Figs. 8 and 9 we show the validation and train accuracy throughout training, respectively. We perform evaluation (i.e., measure train and validation accuracy) once in every 50 rounds for EMNIST and Amazon Reviews, 500 rounds for CIFAR-100, and 1000 rounds for Shakespeare.

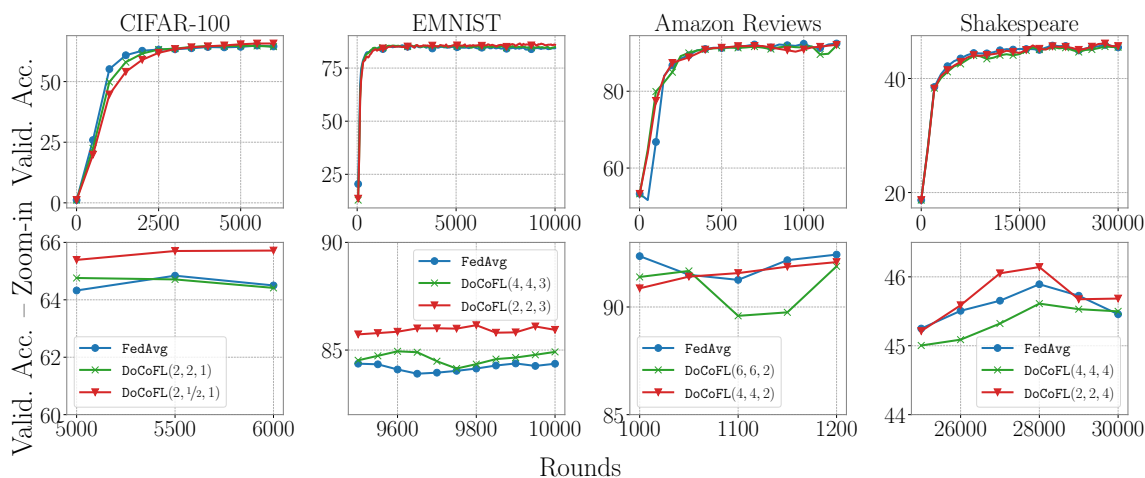


Figure 8: Validation accuracy for different tasks.

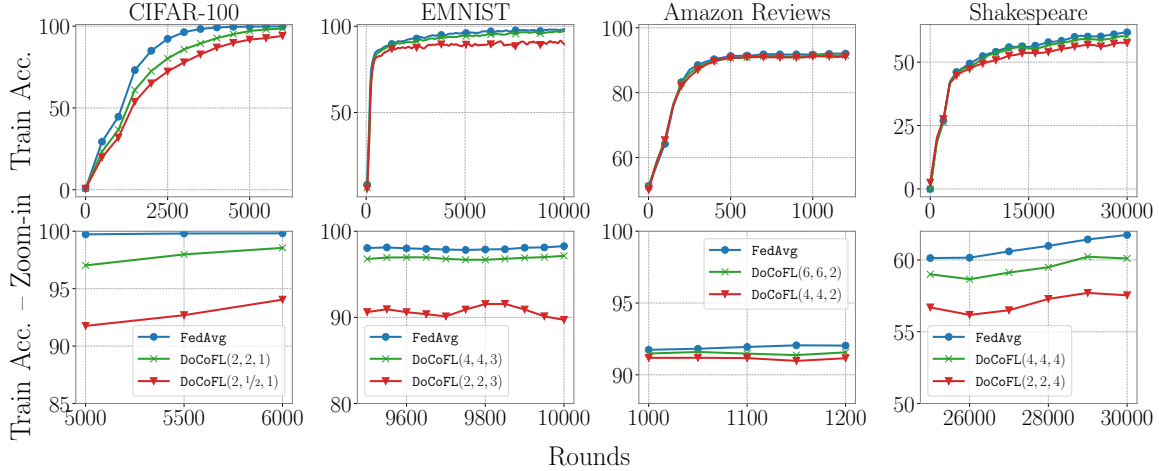


Figure 9: Train accuracy for different tasks.

Following the discussion in §5, Fig. 8 demonstrates that using less bandwidth might help DoCoFL’s generalization ability as it can serve as regularization. For example, consider the EMNIST task, where DoCoFL(2, 2, 3) (i.e., 2 bits per coordinate for anchor and correction compression, and 3 bits per coordinate for uplink compression) outperforms both FedAvg and DoCoFL(4, 4, 3). Unsurprisingly, examining Fig. 9 reveals a reverse image – less bandwidth implies lower train accuracy. These results suggest that using less bandwidth may help in preventing overfitting.